Lithophile and siderophile element systematics of Earth's mantle at the Archean-Proterozoic boundary: Evidence from 2.4 Ga komatiites

I.S. Puchtel[1], M. Touboul[1], J. Blichert-Toft[2], R.J. Walker[1], A.D. Brandon[3], R.W. Nicklas[1], V.S. Kulikov[4], and A.V. Samsonov[5]

[1]Department of Geology, University of Maryland, College Park, MD 20742, USA
[2]Laboratoire de Géologie de Lyon, Ecole Normale Supérieure de Lyon and Université Claude Bernard Lyon 1, CNRS UMR 5276, 46 Allée d'Italie, 69007 Lyon, France
[3]Department of Earth and Atmospheric Sciences, University of Houston, Houston TX, 77004, USA
[4]Institute of Geology, Karelian Research Center RAS, Pushkinskaya Str. 11, 185610 Petrozavodsk, Russia
[5]IGEM Russian Academy of Sciences, Staromonetny 35, Moscow 109017, Russia

Corresponding author:
Igor S. Puchtel. e-mail: ipuchtel@umd.edu

Revised for:
Geochimica et Cosmochimica Acta
Version 2016/02/03

Abstract

New Os isotope and highly siderophile element (HSE) abundance data, in combination with lithophile trace element and Sm-Nd, Lu-Hf, and Hf-W isotope data, are reported for komatiitic basalts from the Vetreny Belt and tonalites from the adjacent Vodla Block in the Fennoscandian Shield. Komatiitic basalts define a Re-Os isochron with an age of 2407±6 Ma and an initial γ^{187}Os = +1.7±0.2 (2SE). The Pt-Os data for chromite separates yield an average initial ε^{186}Os = +0.03±0.02 (2SE). The ^{147}Sm-^{143}Nd and ^{176}Lu-^{176}Hf data for the komatiitic basalts give isochron ages and initial ratios of, respectively, 2403±32 Ma and ε^{143}Nd = −0.90±0.09, and 2451±79 Ma and ε^{176}Hf = +0.4±0.2 (2SE). Bulk tonalites are characterized by average initial γ^{187}Os, ε^{143}Nd, and ε^{176}Hf values of +304±64, +1.8±0.6, and +2.5±1.6 (2SE), respectively, when calculated for the ~3.21 Ga age of the rocks. The komatiitic basalts and tonalites have μ^{142}Nd values of, respectively, +0.5±2.8 and -0.4±5.2 (2SD). By contrast, both the komatiitic basalts and tonalites exhibit positive ^{182}W anomalies of +7.1±4.5 and +12.6±4.5 ppm (2SD), respectively.

The komatiitic basalts were derived from a komatiitic parental magma with ~27 wt.% MgO; it was modified by both assimilation of the tonalites and fractional crystallization *en route* to the surface. Lithophile trace element data constrain the degree of crustal contamination to be 4.0±0.4%. Highly siderophile element abundance data indicate that crustal contamination must have had a negligible effect on the Os isotopic compositions of the komatiitic parental magma. By contrast, the Nd, Hf, and W isotope systematics of the komatiitic parental magma were strongly modified as a result of assimilation of the tonalites. The positive initial ε^{143}Nd and ε^{176}Hf values of the tonalites indicate that they formed via melting of a crustal precursor with time-integrated suprachondritic Sm/Nd and Lu/Hf. This precursor was most likely ancient mafic crust. The large positive ^{182}W anomaly present in the tonalites requires that the precursor crust incorporated a primordial component with Hf/W that became fractionated, relative to the bulk mantle, within the first 50 Ma of Solar System history.

The absolute HSE abundances in the mantle source of the Vetreny komatiite system are estimated to be 66±7% of the present-day Bulk Silicate Earth. This observation, coupled with the normal ^{182}W/^{184}W composition of the komatiitic basalts, when corrected for crustal contamination (μ^{182}W = −0.5±4.5 ppm), indicates that the W-HSE systematics of the Vetreny komatiite system most likely were established as a result of late accretion of chondritic material to Earth. Our present results, combined with isotopic and chemical data available for other early and late Archean komatiite systems, are inconsistent with the model of increasing HSE abundances in komatiitic sources as a result of slow downward mixing into the mantle of chondritic material accreted to Earth throughout the Archean. The observed HSE concentration variations rather reflect sluggish mixing of diverse post-magma ocean domains characterized by variably-fractionated lithophile and siderophile element abundances.

1. Introduction

Despite recent efforts directed towards acquiring combined ^{146,147}Sm-^{142,143}Nd, ^{176}Lu-^{176}Hf, ^{182}Hf-^{182}W, and ^{187}Re,^{190}Pt-^{187,186}Os systematics for Earth's oldest rocks, the available database is still limited, and a number of questions pertaining to the origin and timing of the primordial differentiation and mixing of the mantle, as well as the nature of possible hidden or missing reservoirs, remain unresolved (Chase and Patchett, 1988; Galer and Goldstein, 1991; Blichert-Toft and Albarède, 1997; Rizo *et al.*, 2011, 2013; Willbold *et al.*, 2011, 2015; Touboul *et al.*, 2012, 2014; Puchtel *et al.*, 2013, 2014; Walker *et al.*, 2015).

Chemical and isotopic studies of well-preserved younger rocks may also provide information about early Earth processes. Such work on Paleoproterozoic flood basalts, dike swarms, and mafic layered intrusions worldwide indicates that tremendous volumes of mafic magma, similar to those of Mesozoic flood basalt provinces (Coffin and Eldholm, 1994; Saunders, 2005), were produced on Earth at ~2.45 Ga. Similar ages of the mafic layered intrusions (Alapieti *et al.*, 1990; Balashov *et al.*, 1993; Amelin *et al.*, 1995) and komatiitic lavas (Puchtel *et al.*, 1997) in the Fennoscandian Shield, the Matachewan and Hearst flood basalts and dike swarms (Ciborowski *et al.*, 2015) and the Huronian flood basalts and layered gabbro plutons in the Superior Craton, Canada (Heaman, 1997) suggest that together, these widespread, contemporaneous occurrences of magmatic activity near the Archean-Proterozoic boundary constitute the oldest known large igneous province episode (Heaman, 1997).

This was an important transition period in Earth history. Rapid cooling of the terrestrial mantle is suggested by decreases in both komatiite abundance and MgO contents of komatiite lavas, likely reflecting a fundamental change in heat flux at the core-mantle boundary (Campbell and Griffiths, 1992; Nisbet *et al.*, 1993; Herzberg *et al.*, 2010), stabilization of major cratons (Condie, 1986), onset of plate tectonics in its present form (Brown, 2006), and the rise of oxygen in Earth's atmosphere, as manifested

by the worldwide occurrence of banded iron formations of this age (Barley *et al.*, 1997) and the disappearance of mass-independent fractionation of sulfur (Farquhar *et al.*, 2000). Hence, if this series of massive volcanic events does indeed signify a major transition in Earth history, it is plausible that deep mantle-derived rocks, such as komatiites, from this period can reveal important information about the chemical and thermal evolution of the Earth.

The geological record during this crucial period in Earth history, however, remains fragmentary, and the komatiite record is particularly limited. The remarkably well-preserved supracrustal sequences of the 2.41-2.44 Ga Vetreny Belt in the Fennoscandian Shield are a rare exception to this. Here, we present new Re-Os and Pt-Os isotopic and highly siderophile element (HSE, including Re, Os, Ir, Ru, Pt, and Pd) abundance data, as well as ^{146,147}Sm-^{142,143}Nd, ^{176}Lu-^{176}Hf, and ^{182}Hf-^{182}W isotopic and lithophile trace element data, for 2.41 Ga komatiitic basalt lavas from Victoria's lava lake, as well as for ~3.21 Ga tonalites of the adjacent Vodla Block. In studying these rocks, the main objective was to interrogate the chemical and isotopic composition of the mantle at the Archean-Proterozoic boundary, with the expectation of identifying isotopic signatures of mantle reservoirs that may have survived from the earliest stages of Earth's differentiation history.

2. Geological background, samples, and previous studies

The 250 km long Paleoproterozoic Vetreny Belt in SE Fennoscandia is considered to be part of the oldest known large igneous province that formed in a continental rift setting, during the interaction of a mantle plume with the Archean continental crust of the Karelian granite-greenstone terrain (Heaman, 1997; Puchtel *et al.*, 1997; Kulikov *et al.*, 2010).

Lithophile trace element and Sm-Nd isotopic studies have shown that magmas parental to the Vetreny Belt lavas were komatiitic in composition and were derived from a long-term LREE-depleted mantle source (Puchtel *et al.*, 1997). These authors concluded that the chemical evolution of these

113 komatiite magmas *en route* to the surface was controlled by a combination of ~50% fractional
114 crystallization and 4–15% assimilation of felsic crustal rocks from the adjacent ~3.2 Ga Vodla Block.
115 Puchtel *et al.* (1997) reported internal Sm–Nd isochron ages of 2449±35 and 2410±34 Ma, and a bulk-
116 rock Pb–Pb isochron age of 2424±178 Ma, for the uppermost Vetreny suite komatiitic basalts, and a U–
117 Pb zircon age of 2437±3 Ma for the stratigraphically lowermost Kirichi suite andesites and basalts.
118 Rocks from the Victoria's lava lake, which is part of the Vetreny suite, are the primary focus of this
119 study. The lava lake consists of a ~110 m-deep sequence of komatiitic basalt, which filled a large
120 topographic depression following eruption and has been estimated to have erupted with *ca.* 15 wt.%
121 MgO (Puchtel *et al.*, 1996). After emplacement, the lava lake underwent differentiation and developed a
122 prominent internal layered structure comprised of three main units (from the top down): an upper chilled
123 margin, a spinifex zone, and a cumulate zone (**Fig. 1**). The rocks are in a superb state of preservation;
124 the metamorphic grade did not exceed prehnite-pumpellyite facies.
125 Puchtel *et al.* (2001) reported a Re–Os isochron age of 2384±57 Ma and a chondritic, albeit
126 imprecise, initial γ^{187}Os = +0.3±1.1 (2SE) for a set of four cumulate samples and two chromite separates
127 from the lava lake. Platinum-group element (PGE: Os, Ir, Ru, Pt, and Pd) abundances for a set of whole-
128 rock samples and mineral separates were obtained by Puchtel and Humayun (2001) using the NiS fire
129 assay digestion method, combined with the isotope dilution inductively-coupled plasma mass-
130 spectrometry (ID ICP-MS) technique. This digestion method, however, was later shown to be inefficient
131 at achieving complete sample-spike equilibration (Puchtel *et al.*, 2004b). As a result, concentrations of
132 most PGE, especially Os, Ir, and Ru, were likely under-determined by as much as 50%.
133 For this study, we collected a new set of samples across several sections of the lava lake, including
134 those studied earlier by (Puchtel *et al.*, 1996), as well as from those that had not been previously
135 sampled. The locations of the samples are shown on the integrated section of the lava lake in **Fig. 1**. The

136 purpose of the new sampling campaign was to (1) collect samples large enough to separate pure olivine
137 and chromite in quantities sufficient for both high-precision Os isotopic analysis and minor element and
138 HSE abundance determinations; (2) obtain new, high-quality material suitable for W isotopic analysis
139 using metal-free equipment previously not available; and (3) obtain high-precision Re-Os, Pt-Os, Hf-W,
140 Sm-Nd, and Lu-Hf isotopic and lithophile trace element, W, and HSE abundance data, using state-of-
141 the-art analytical techniques, in order to constrain the lithophile and siderophile element compositions of
142 the mantle at the Archean-Proterozoic boundary.

143 We also analyzed four representative tonalite samples from the tonalite-trondhjemite-granodiorite
144 (TTG) complex of the Vodla Block in order to assess effects of crustal contamination on the Os, W, Nd,
145 and Hf isotope systematics of the Victoria's lava lake komatiitic basalts. Detailed information on
146 location of the samples, trace element geochemistry, and Sm-Nd and U-Pb zircon chronology for the
147 tonalites can be found in Kulikov *et al.* (1990), Kulikova (1993), Lobach-Zhuchenko *et al.* (1993) and
148 Chekulaev *et al.* (2009). Geochemically, the tonalites are characterized by high Al_2O_3, high Na_2O/K_2O,
149 and $(La/Yb)_N$ >30 that are similar to other tonalites from the Fennoscandian Shield, such as those from
150 the 3.1 Ga TTG complexes of southeastern Karelia and northern Finland (Jahn *et al.*, 1984), and the 2.85
151 and 2.65 Ga TTG suite of eastern Finland (Martin *et al.*, 1983). These rocks have T_{DM} Nd model ages of
152 3288±94 Ma (2SE, N = 9) and a U-Pb SHRIMP zircon age of 3213±32 Ma (Kulikov *et al.*, 1990;
153 Chekulaev *et al.*, 2009).

154 3. Analytical techniques

155 3.1. Sample preparation and mineral separation

156 Each sample, from 2 kg (chilled margin and spinifex-textured lavas) to 20 kg (cumulates) in weight, was collected from
157 the surface outcrops in the form of multiple pieces of rock using either a sledge hammer or rock saw. Any visible alteration
158 was either avoided or removed at the sample collection stage. In order to assess the extent of chemical homogeneity of the
159 samples, the collected material for some of the cumulate samples was split in halves (designated parts A and B), and each

half was processed as a separate sample. After removing any sledge hammer marks using sand paper, pieces of rock were crushed in an alumina-faced jaw crusher. A 200-g aliquot of each crushed sample was ground in an alumina shatter box and then finely re-ground in an alumina-faced disk mill. This ground material was further used for the chemical studies. Remaining crushes of the cumulate samples were subsequently used for mineral separation.

Pure olivine and chromite separates were obtained at the Institute of Geology in Petrozavodsk using the combination of heavy liquid and magnetic separation techniques and handpicking.

3.2. Major, minor, and trace elements

Major and minor element analyses were carried out at the Franklin and Marshall College on fused glass discs using a Phillips 2404 XRF vacuum spectrometer and following the protocol of Mertzman (2000). Typical accuracy of the analyses was ~1% relative for major elements present in concentrations >0.5% and ~5% relative for the rest of the major and the minor elements (2SD), as reported by Mertzman (2000) and indicated by the analysis of the USGS standard reference materials (SRM) BIR-1 and BCR-1 as unknowns (**Table 1A** of the Appendix).

The abundances of the lithophile trace elements and transition metals were determined using the standard addition solution inductively-coupled plasma mass-spectrometry technique (SA ICP-MS). Between 25 and 35 mg of sample powder were weighed out in 15 mL screw-cap Savillex Teflon vials. Approximately 0.5 mL double-distilled conc. HNO_3 and 3 mL double-distilled conc. HF were added, the vials were sealed and kept on a hotplate at 200ºC for 48 hours. The vials were then opened, the sample solutions evaporated to dryness, 0.5 mL of distilled SeaStar conc. $HClO_4$ added to the dry residue to convert fluorides into perchlorates, the vials sealed again and kept on a hotplate at 200ºC for 48 hours. The vials were re-opened and the sample solutions dried down on the hotplate at 230ºC. This step was followed by re-dissolution of the residue in 2 mL of 6*M* HCl to convert it into the chloride form. This step was repeated. The dry residue was taken up in ~10 grams of 0.8*M* HNO_3 (with the exact weight recorded), and this stock solution was used for preparing spiked aliquots used for ICP-MS measurements. Two standard addition spikes were prepared, one containing concentrated mixed solutions of Sc, Cu, Co, Ga, Y, and Zr, and the other containing Nb, Hf, Th, U, and REE. Three aliquots of each sample, each containing ~1.0 gram of sample stock solution (with the exact weight recorded), were prepared for each of the two groups of the elements to be analyzed, one containing no spike, one with the amount of spike containing 2× the estimated amount of element present in the sample aliquot, and one with the amount of spike containing 4× the estimated amount of element present in the sample aliquot, with the exact weights of the spike recorded. One total analytical blank (TAB) was also prepared and measured with every batch of six samples. Approximately 100 mg of 500 ppb In solution was added to each sample aliquot and the TAB solutions to monitor and correct for signal drift during analysis, and the one sample- and two sample-spike solutions for each sample were diluted to 10 grams with 0.8*M* HNO_3.

The sample solutions were analyzed on a *ThermoFisher Element2* sector field ICP-MS at the *Plasma Laboratory, University of Maryland*. Prior to analysis, the instrument was thoroughly tuned to maximize sensitivity and minimize oxide production and mass-calibrated. The intensities of selected isotopes of each element were measured in either low resolution (trace elements) or medium resolution (transition metals) modes. The raw data were reduced using an in-house Excel macro. The in-run uncertainties on the concentrations were typically better than 1% for all elements (2SE). The accuracy and precision of the analyses were determined via replicate analysis of the USGS SRM BIR-1 and BCR-1 (**Table 1A**); for most elements, it was ~5% (2SD), which includes the uncertainty introduced by the SRM powder heterogeneity.

3.3. Highly Siderophile Elements

3.3.1. Re-Os isotopic and HSE abundance data. To obtain the Re-Os isotopic and HSE abundance data, 1.4-1.7 g of whole-rock powder, 0.8-1.1 g of pure olivine separate, and 0.04-0.05 g of pure chromite separate, 6 mL of Os-purged, triple-distilled conc. HNO_3, 4 mL of triple-distilled conc. HCl, and appropriate amounts of mixed ^{185}Re-^{190}Os and HSE (^{99}Ru,^{105}Pd,^{191}Ir,^{194}Pt) spikes were sealed in double internally-cleaned, chilled 25 mL Pyrex™ borosilicate Carius Tubes (CT) and heated to 270°C for 96 h. Osmium was extracted from the acid solution by CCl_4 solvent extraction (Cohen and Waters, 1996), then back-extracted into HBr and purified via microdistillation (Birck *et al.*, 1997). Ruthenium, Pd, Re, Ir, and Pt were separated and purified using anion exchange chromatography following the protocol of Rehkämper and Halliday (1997) with some modifications. Average total analytical blank (TAB) during the analytical campaign was (in pg): Ru 1.1±0.5 (2SE, N = 5), Pd 6±2, Re 0.43±0.17, Os 0.19±0.05, Ir 0.45±0.23, and Pt 11±5. For the whole-rock komatiitic basalt samples, the TAB for all HSE constituted less than 0.1% of the total element analyzed. For the olivine and chromite separates, the TAB for Os constituted less than 0.2%, for Ir and Ru less than 0.4%, for Re between 2% and 26%, for Pt between 0.4 and 5%, and for Pd between 0.5 and 12% of the total element analyzed. For the tonalities, the TAB constituted 0.3-1% for Re, 3-6 for Os, 8-10% for Ir, 40-100% for Ru, 9-28% for Pt, and 4-27% for Pd, of the total element analyzed.

Osmium isotopic measurements were done *via* negative thermal ionization mass-spectrometry (*N-TIMS:* Creaser *et al.*, 1991). All samples were analyzed using a secondary electron multiplier (SEM) detector of a *ThermoFisher Triton*® mass spectrometer at the *Isotope Geochemistry Laboratory (IGL),*University of Maryland. The measured isotopic ratios were corrected for mass-fractionation using ^{192}Os/^{188}Os = 3.083. The internal precision of measured ^{187}Os/^{188}Os for all samples was between 0.03% and 0.07% relative (2SE). The ^{187}Os/^{188}Os ratio of 300-500 pg loads of the in-house Johnson-Matthey Os standard measured during the period of the analytical campaign averaged 0.11376±10 (2SD, N = 64). This value characterizes the external precision of the isotopic analysis (0.1%), which we used to calculate the true uncertainty on the measured ^{187}Os/^{188}Os ratio for each individual sample. The measured ^{187}Os/^{188}Os ratios were further corrected for instrumental bias relative to the average ^{187}Os/^{188}Os = 0.11379 measured for the Johnson-Matthey Os standard on the Faraday cups of the *IGL Triton*. The correction factor of 1.00026 was calculated by dividing this value by the average ^{187}Os/^{188}Os measured for the Johnson-Matthey Os standard on the SEM of the same instrument.

The measurements of Ru, Pd, Re, Ir, and Pt were performed at the *Plasma Laboratory* via inductively-coupled plasma mass-spectrometry (ICP-MS) using a *Nu Plasma* instrument with a triple electron multiplier configuration in static mode. Isotopic mass-fractionation was monitored and corrected for by interspersing samples and standards. The accuracy of the data was assessed by comparing the results for the reference materials UB-N and GP-13 obtained during the ongoing analytical campaign with results from other laboratories. Concentrations of all HSE and Os isotopic compositions obtained at the *IGL* are in good agreement with data from other laboratories, as reported in Puchtel *et al.* (2014). Diluted spiked aliquots of iron meteorites were run during each analytical session as secondary standards. The results from these runs agreed within 0.5% for Re and Ir, and within 2% for Ru, Pt, and Pd, with fractionation-corrected values obtained from measurements of undiluted solutions of iron meteorites using Faraday cups of the same instrument with a signal of >100 mV for the minor isotopes. We therefore cite ±2% as the uncertainty on the concentrations of Ru, Pt, and Pd, ±0.5% as the uncertainty on the concentrations of Re and Ir, and ±0.1% as the uncertainty on the concentrations of Os for the whole-rock komatiitic basalt samples. For the whole-rock tonalite samples, the uncertainties on the HSE concentrations were largely determined by the uncertainty on the

variations in the TAB and were 0.5% for Re, 2-3% for Os, up to 50% for Ru, and between 2 and 14% for Pt and Pd. For the olivine and chromite separates, the uncertainties on the Os, Ir, and Ru abundances were the same as for the whole-rock samples, whereas the uncertainties on the Re concentrations were between 1% and 13%, on the Pt concentrations between 2% and 3%, and on the Pd concentrations between 2% and 6%, assuming a ~50% variation in abundances of the TAB. The uncertainty on the Re concentration was the main source of uncertainty on the Re/Os ratio. For the whole-rock samples, this uncertainty was estimated to be 0.5%, and for the olivine and chromite separates between 1% and 13%.

All regression calculations were performed using ISOPLOT 3.00 (Ludwig, 2003). The uncertainties on the concentrations and isotopic ratios used for the regression calculations are those stated above. The initial $\gamma^{187}Os$ values were calculated as the per cent deviation of the isotopic composition at the time defined by the isochron relative to the chondritic reference of Shirey and Walker (1998) at that time.

The average chondritic Os isotopic composition at the time defined by the isochron was calculated using the ^{187}Re decay constant $\lambda = 1.666 \times 10^{-11}$ year^{-1}, an early Solar System initial $^{187}Os/^{188}Os = 0.09531$ at $T = 4558$ Ma, and $^{187}Re/^{188}Os = 0.40186$ (Smoliar *et al.*, 1996; Shirey and Walker, 1998).

3.3.2. Pt-Os isotopic data. In the present study, we followed the methodology developed by Puchtel *et al.* (2004a) for determining precise initial $^{186}Os/^{188}Os$ and $^{187}Os/^{188}Os$ isotopic compositions in materials requiring corrections for the in-growth of radiogenic ^{186}Os and ^{187}Os, such as Archean komatiites. This methodology involves simultaneous high-precision determination of $^{186}Os/^{188}Os$ and $^{187}Os/^{188}Os$ ratios on unspiked digestions combined with determination of elemental abundance ratios of Pt, Re, and Os on small aliquots taken from the unspiked digestions to ensure the representativeness of these ratios for each sample digestion. In order to obtain the amount of Os required for high-precision measurements of $^{186}Os/^{188}Os$ and $^{187}Os/^{188}Os$ (~100 ng), between 2 and 12 grams of pure chromite separates from cumulate samples 01001, 01105, 12001, and 12105 were digested in 2 to 8 CT. For the initial unspiked digestions, ~1.5 g of a chromite separate, 9 mL of double-purged, triple-distilled conc. HNO_3, and 6 mL of triple-distilled conc. HCl were placed into a double internally cleaned, 38 mL Pyrex™ CT chilled to 0°C, sealed and kept in an oven at 270°C for 96 hours. After the digestion was complete, the tubes were chilled and opened and ~0.25 mL of the acid sample solution from each CT in the batch of CT(s) representing a single sample digestion were transferred into a 25 mL Pyrex™ CT for precise determination of Pt/Os, Re/Os, and Ir/Os (for monitoring potential Os losses during the aliquot transfer). Before the transfer procedure, the double internally cleaned, 25 mL Pyrex™ CT was chilled to 0°C and appropriate amounts of the mixed ^{185}Re-^{190}Os and HSE spikes were added to it, followed by 4 mL of triple-distilled conc. HNO_3 and 3 mL of triple-distilled conc. HCl after the sample solution transfer was completed. The sealed CT with the spiked sample solutions were kept in the oven at 270°C for 24 h to achieve sample-spike equilibration. After opening the CT, the spiked aliquots were processed using the same procedure utilized for the Re-Os and HSE analyses. From the remaining part of the unspiked acid sample solutions, Os was extracted and purified using the same protocol utilized for the Re-Os work. The Os cuts from the batch of CT containing a single sample were combined into one cut and used for the precise measurements of $^{186}Os/^{188}Os$ and $^{187}Os/^{188}Os$.

Measurements of Re, Os, Pt, and Ir isotopic compositions from the spiked aliquots, for the determination of precise Re/Os, Pt/Os, and Ir/Os ratios, were performed using the same protocol as that employed in the Re-Os and HSE study described above.

The high-precision measurements of the $^{186}Os/^{188}Os$ and $^{187}Os/^{188}Os$ ratios were performed by *N-TIMS* in static mode on a *ThermoFisher Triton®* mass spectrometers at either the NASA Johnson Space Center (*JSC*) or the *IGL*. Signals of >100 mV on mass 234 ($^{186}Os^{16}O_3^-$) and 235 ($^{187}Os^{16}O_3^-$) were generated to reach the maximum in-run precisions for the $^{186}Os/^{188}Os$ and $^{187}Os/^{188}Os$ ratios. During each run, between 720 and 1440 ratios were collected for each sample load; the in-run uncertainties on the measured $^{186}Os/^{188}Os$ and $^{187}Os/^{188}Os$ ratios are quoted as 2SE. The possible isobaric interference of $^{186}W^{16}O_3^-$ on $^{186}Os^{16}O_3^-$ was assessed by measuring $^{184}Os/^{188}Os$ (modified if $^{184}W^{16}O_3^-$ present) and monitoring mass 231 ($^{183}W^{16}O_3^-$) using the electron multiplier. Although a signal of ~3-10 cps was normally measured at mass 231, its size in comparison to other potential isotopes of W indicated that it was not W, and, therefore, no W corrections were made. Instead, the small signals typically observed at mass 231 are consistent with the expected amount of $^{198}Pt^{16}O^{17}O$ produced from the Pt filaments during ionization. This was indicated from the mass scan profiles from mass 226 ($^{194}Pt^{16}O_2$) to mass 230 ($^{198}Pt^{16}O_2$), which clearly showed all of the PtO_2 isotopes in their expected proportions in the spectrum, and no evidence for WO_3 production at mass 230 or 231.

The mean of the Johnson-Matthey Os standard runs during the period of data collection was 0.001307±5 and 0.001308±10 for $^{184}Os/^{188}Os$, 0.1198462±21 (±18 ppm) and 0.1198447±16 (±14 ppm) for $^{186}Os/^{188}Os$, and 0.113789±4 and 0.113791±3 for $^{187}Os/^{188}Os$ at the *JSC* (2SD, $N = 23$) and at the *IGL* (2SD, $N = 14$), respectively. We used these values to assess the true uncertainty on the measured $^{186}Os/^{188}Os$ ratios for individual samples, and also to calculate the uncertainty on the average initial $^{186}Os/^{188}Os$ ratio. Since the high-precision $^{186}Os/^{188}Os$ ratios obtained at *JSC* and *IGL* were previously instrumental bias-corrected to a common JM Os standard $^{186}Os/^{188}Os$ value of 0.1198475 (Puchtel *et al.*, 2009b), the $^{186}Os/^{188}Os$ ratios measured in this study were also instrumental bias-corrected to $^{186}Os/^{188}Os = 0.1198475$ using correction coefficients of 1.0000110 and 1.0000237 at *JSC* and *IGL*, respectively. To calculate the initial $^{186}Os/^{188}Os$ ratios, the Pt/Os ratios obtained from the spiked runs and the ^{190}Pt decay constant $\lambda = 1.477 \times 10^{-12}$ year^{-1} (Begemann *et al.*, 2001) were used. The initial $\varepsilon^{186}Os$ values were calculated as parts per 10,000 deviation of the $^{186}Os/^{188}Os$ ratio of the sample at the time of lava emplacement relative to the chondritic reference of Brandon *et al.* (2006) at that time using an early Solar System initial $^{186}Os/^{188}Os = 0.1198269$ at $T = 4567$ Ma and $^{190}Pt/^{188}Os = 0.00174$.

3.4. W isotopic compositions and abundances

In order to determine W isotopic compositions and abundances, the techniques developed by Touboul and Walker (2012) were utilized. Between 10 and 35 g of sample powder were processed to obtain ~1.0 μg of W necessary for acquiring high-precision W isotopic data for each sample. Powder aliquots were digested in 120 mL Teflon vials using a 5:1 mixture of conc. HF and HNO_3 over the course of a week at 150ºC. After evaporation to dryness, residues were digested twice in concentrated HNO_3, with traces of H_2O_2, for ~24 hours at 120ºC, and dried down. Residues were then converted into the chloride form by repeated dissolutions in 6 *M* HCl and subsequent dry downs. The residues were finally re-dissolved in 10 to 40 mL of a mixture of 1.0 *M* HCl+0.1 *M* HF. After centrifugation, W of the supernatant was extracted and purified using a four-stage ion exchange chromatography protocol that allows for efficient extraction and purification of W from large samples. Tungsten recovery using this procedure was better than 90% for all samples analyzed.

Tungsten isotope measurements were performed *via N-TIMS* using the *ThermoFisher Triton®* at the *IGL*. This analytical technique permitted achievement of a ±4.5 ppm external precision (2SD) on the $^{182}W/^{184}W$ ratio. TAB averaged ~1.8 ng, and

306 was less than 0.2% of the total W present in the analyzed W cuts. Blank corrections on the measured W isotope composition
307 were, therefore, negligible.
308 Tungsten abundances were determined by isotope dilution ICP-MS using a ^{182}W-enriched spike. Powder aliquots of 100-
309 200 mg were digested in 15 mL screw-cap Teflon vials using a 5:1 mixture of conc. HF and HNO_3 at 180ºC for 3 to 4 days,
310 followed by evaporation to dryness. Residues were treated twice with HNO_3 and traces of H_2O_2 at 120ºC for ~24 h. After
311 complete drydown, residues were converted into the chloride form by adding 6 *M* HCl, followed by another drydown.
312 Residues were then equilibrated with 6 *M* HCl+0.01 *M* HF at 120ºC for ~24 h, whereupon complete dissolution was normally
313 achieved. Finally, solutions were dried down and residues re-dissolved in 2ml of mixtire of 0.5 *M* HCl+0.5 *M* HF, and W was
314 purified using a previously established anion exchange chromatography technique (*e.g.,* Kleine *et al.*, 2004).
315 The isotopic composition of the sample-spike mixtures were measured using the *Nu Plasma* ICP-MS at the *Plasma*
316 *Laboratory*. The TAB for W averaged 170±50 pg, corresponding to contributions of <1% of the total W present in the
317 samples.

318 **3.5. Sm-Nd isotopic compositions and abundances**

319 The Sm-Nd isotopic studies were carried out at the *IGL* following the technique of Boyet and Carlson (2005) with some
320 modifications (Puchtel *et al.*, 2013). Approximately 200 mg of sample powder were sealed in a screw-cap 15 mL Teflon
321 vessel with 3 mL of conc. HF and 0.5 mL of conc. HNO_3 and digested on a hotplate at 200°C for 48 h. The vessels were
322 opened, the solutions dried down, 0.5 mL of conc. $HClO_4$ were added, the vials sealed and kept on a hotplate at 200°C for 48
323 h. The solutions were then dried down at ~230°C, and the residues converted into the chloride form using 6 *M* HCl. This step
324 was repeated. After the final dry down, the residue was taken up in 2.5 *M* HCl and a 5% aliquot of the solution was collected
325 and used for determination of the Sm and Nd concentrations *via* the SA ICP-MS technique. From the remaining 95% sample
326 solution, the rare earth elements (REE) were first separated using standard cation exchange chromatography. The Nd
327 fractions were then separated from the other REEs and purified using first 2-methyllactic acid cation exchange
328 chromatography and then HDEHP extraction chromatography. The resultant Nd cuts were used for high-precision
329 measurements of the Nd isotopic compositions.
330 High-precision measurements of Nd isotopic compositions were performed at the *IGL* on the *ThermoFisher Triton* mass-
331 spectrometer, using a two-line acquisition scheme and a multi-dynamic routine. For each sample load, between 2400 and
332 3600 ratios were collected with 8 sec. integration times in blocks of 20 ratios. For every three blocks of data collection, the
333 two peaks were centered, the ion beam was re-focused, and the amplifiers were electronically rotated relative to the Faraday
334 cup detectors. A 30 sec. baseline measurement *per* block was performed for each Faraday cup/amplifier pair by beam
335 deflection. The effects of mass-fractionation were corrected for using an exponential law, *via* normalizing to ^{146}Nd/^{144}Nd =
336 0.7219. A total of ten loads of 900 ng of the Nd standard AMES were run at the beginning and end of the analytical session,
337 with 2400 ratios collected during each measurement. During the measurements, the signal intensities for both the standards
338 and the samples were kept at constant levels, between 3V and 5V on mass 142. The calculated ^{147}Sm/^{144}Nd ratios were
339 between 10^{-5} and 10^{-6}, meaning that corrections for Sm isobaric interferences were negligible. The calculated ^{142}Ce/^{142}Nd
340 ratios were between 10^{-5} and 10^{-4}, resulting in interference corrections of >10 ppm on the ^{142}Nd/^{144}Nd ratio in some samples.
341 No correlation between measured ^{142}Nd/^{144}Nd and the intensity of the ^{140}Ce signal was observed, however, indicating that
342 these interferences were adequately corrected for. During the course of the analytical campaign, the external reproducibility

of the Nd standard measurements was ±2.8 ppm for the $^{142}Nd/^{144}Nd$ ratio and ±3.5 ppm for the $^{143}Nd/^{144}Nd$ ratio (2SD, N = 34). The $^{142}Nd/^{144}Nd$ ratios are expressed in $\mu^{142}Nd$ units calculated as parts per million (ppm) deviation from the average $^{142}Nd/^{144}Nd$ ratio of the Nd standard AMES run during the course of the entire analytical campaign.

The $^{147}Sm/^{144}Nd$ ratios used for calculating the initial $^{143}Nd/^{144}Nd$ isotopic ratios, were determined using the SA ICP-MS technique. The uncertainty on this ratio was determined from the analysis of multiple aliquots of the USGS SRM BIR-1 to be ±0.5% relative (2SD).

3.6. Lu-Hf isotopic compositions and abundances

The Lu-Hf isotopic measurements were carried out at the *Ecole Normale Supérieure* (*ENSL*) in Lyon, France. The sample dissolution procedure, employing Parr bombs and a mixed >98% pure ^{176}Lu-^{180}Hf spike, and the Lu and Hf separation protocols used are described in Blichert-Toft *et al.* (1997), Blichert-Toft (2001), and Blichert-Toft and Puchtel (2010). Lutetium and Hf isotopic compositions were measured by multi-collector ICP-MS using a *Nu Plasma 500 HR* coupled with a desolvating nebulizer *DSN-100* and following the protocols of Blichert-Toft *et al.* (1997, 2002). The JMC-475 Hf standard was analyzed between every two to three samples and gave an average $^{176}Hf/^{177}Hf$ = 0.282164±0.000010 (2SD; N = 8), which represents the most accurate estimate of the external precision of the Hf isotopic analyses (0.0035%). Since this value is identical, within error, to the accepted value for the JMC-475 Hf standard of 0.282163 ± 0.000009 (Blichert-Toft *et al.*, 1997), no correction was applied to the data. We used the uncertainty obtained from the external reproducibility of the Hf standard as the uncertainty on the Hf isotopic composition for the isochron calculations, as all in-run precisions were either better or equal to the external precision. The uncertainty on the $^{176}Lu/^{177}Hf$ ratio, as measured by isotope dilution, was 0.2% and this is the value we used for the isochron calculations. TAB was <20 pg for both Lu and Hf.

For the isochron calculations, ISOPLOT 3.00 (Ludwig, 2003) and the ^{176}Lu decay constant of 1.867×10^{-11} $year^{-1}$ (Scherer *et al.*, 2001; Söderlund *et al.*, 2004) were used. The $\varepsilon^{176}Hf$ values were calculated as parts per 10,000 deviation of the $^{176}Hf/^{177}Hf$ of the lavas at the time of their formation relative to that of the chondritic reference at that time defined as $^{176}Lu/^{177}Hf$ = 0.0336 and $^{176}Hf/^{177}Hf$ = 0.282785 (Bouvier et al., 2008).

4. Results

4.1. Major, minor, and trace element data

The new major, minor, and trace element data for the whole-rock samples and olivine separates from the Victoria's lava lake are presented in **Table 1A;** selected minor and trace element data are plotted on elemental variation diagrams in **Fig. 2** and as BSE-normalized values in **Fig. 3**. The top of the upper chilled margin (samples 01110/1 and 12110/1) with an average MgO content of 15 wt.%, which experienced no fractionation after lava emplacement, most likely represents the composition of the

374 emplaced lava (Puchtel *et al.*, 1996). Concentrations of major, minor, and trace elements vary
375 systematically across the lava lake in a manner similar to that of thick differentiated komatiitic lava
376 flows, such as Fred's Flow in Ontario, Canada (e.g., Arndt, 1977). The MgO contents are nearly
377 constant in the upper ~20 m of the lava lake, then drop first to 9-11 wt.% in the pyroxene spinifex zone,
378 and then further to 7-8 wt.% in the subzone of fine- to coarse-grained basalt at the bottom of the spinifex
379 zone. They increase again in the cumulate zone, reaching a maximum of ca. 27 wt.% in the upper half of
380 the cumulate zone, and then decrease to ca. 20 wt.% near the bottom. When plotted against MgO,
381 incompatible major, minor, and lithophile trace elements define well-constrained trends with negative
382 slopes intersecting the MgO axis at 47.5±1.0 wt.% (2SE) (**Fig. 2**). This is consistent with the average
383 MgO contents of cores of olivine microphenocrysts from the upper chilled margin of the lava lake of
384 48.1 wt.% (Puchtel *et al.*, 1996). These observations indicate that the trends represent olivine control
385 lines, and attest to the immobile behavior of these elements during alteration.
386 The bulk olivine separates analyzed in this study also plot on the liquid lines of descent. These,
387 however, contain only between 42-46 wt.% MgO, indicating the presence, together with liquidus
388 olivine, of a small proportion of olivine that crystallized from a more evolved liquid, as well as of
389 variable amounts of interstitial liquid within the grains.
390 The Ni vs. MgO abundance data for the lava lake samples define a trend with a positive slope,
391 testifying to the typical compatible behavior of Ni during komatiite differentiation (**Fig. 2**). Regression
392 of the Ni concentration data against the abundance data for the elements that are incompatible with
393 olivine gives an average intercept at 2277±27 ppm Ni, which corresponds to the average Ni content in
394 the bulk fractionating mineral assemblage. Since the Ni variations in the lava lake were entirely
395 controlled by olivine, as evidenced by the liquid line of descent for Ni passing through the olivine
396 compositions (**Fig. 2**), this value further represents the mean Ni content in the average liquidus olivine.

Chromium abundances in the whole-rock samples show strong positive correlation with MgO content (**Fig. 2**), indicating that Cr was predominantly controlled by fractionation of 1-2% liquidus chromite. The olivine separates plot well below this trend indicating incompatible behavior of Cr in the olivine, with a $D^{ol\text{-}liq}_{Cr}$ well below unity.

The average Al_2O_3/TiO_2 = 19.5±0.3 of the lava lake is essentially identical to that of the Munro Township komatiites (Puchtel *et al.*, 2009b), which is consistent with the previous (Puchtel *et al.*, 1996) classification of the lava lake as belonging to the Al-undepleted, or Munro-type, lavas of Nesbitt and Sun (1976). The lavas are moderately enriched in highly incompatible lithophile trace elements (**Fig. 3**), such as light REE, Th, and U ($(La/Sm)_N$ = 2.19±0.02, 2SE), somewhat depleted in heavy REE ($(Gd/Yb)_N$ = 1.32±0.01), and are characterized by strong negative Nb anomalies (Nb/Nb* = 0.29±0.01).

Tonalites of the Vodla Block analyzed in this study contain 66-71 wt.% SiO_2 and 16-18 wt.% Al_2O_3 (**Table 1A**), consistent with the major element data reported for Vodla Block tonalites by Kulikov *et al.* (1990) and Lobach-Zhuchenko *et al.* (1993), and the classification of these rocks as typical high-Al Archean tonalites. The rocks are moderately to strongly enriched in highly incompatible lithophile trace elements (**Fig. 3**), show variable REE patterns from strongly fractionated with low heavy REE concentrations ($(La/Sm)_N$ = 7.1–8.5, $(Gd/Yb)_N$ = 3.6–3.8), to moderately fractionated with medium heavy REE concentrations ($(La/Sm)_N$ = 4.3, $(Gd/Yb)_N$ = 2.0), and exhibit strong negative Nb anomalies (Nb/Nb* = 0.10-0.18). The rocks are characterized by variable both positive and negative Eu anomalies (Eu/Eu* = 0.78 – 1.6), likely as a result of Eu mobility during alteration and amphibolites facies metamorphism.

4.2. HSE abundance data

The HSE abundances of the whole-rock samples and olivine and chromite separates obtained in this study are presented in **Table 1** and plotted in **Figs. 4** and **5**. All HSE, including Re, have been previously

shown to be immobile during alteration of the lava lake (Puchtel *et al.*, 2001; Puchtel and Humayun, 2001). This conclusion is consistent with the strong correlation observed between Re, the most fluid-mobile element among the HSE, and MgO, for the new samples analyzed in this study (**Fig. 5**), which all plot on a trend that coincides with the olivine control line.

Both olivine and chromite separates exhibit typical dome-shaped CI chondrite-normalized HSE patterns, with a maximum at Ru (**Fig. 4)**. Ruthenium concentrations are remarkably uniform within both olivine and chromite separates (4.9±0.3 and 341±14 ppb, respectively), and there is a nearly two orders of magnitude difference in absolute concentrations between the two phases. In addition, olivine and chromite separates are characterized by subchondritic $(Os/Ir)_N$ = 0.70±0.09 and 0.59±0.01, respectively.

The upper chilled margin samples, which represent the composition of the emplaced komatiitic basalt lava (Puchtel *et al.*, 1996), contain ~0.20 ppb Os, 0.46 ppb Re, and 13 ppb Pt, and exhibit fractionated HSE patterns with $(Pd/Ir)_N$ = 20±3 and strongly subchondritic $(Os/Ir)_N$ = 0.40±0.05. Osmium, Ir, and Ru show a broad pattern of increasing abundances with increasing MgO contents in samples collected between the upper chilled margin and the cumulate zone, typical of the so-called Munro-type lavas (**Fig. 5**). In the cumulate zone, however, both Os and Ir behaved incompatibly, showing a pattern of decreasing abundances with increasing MgO content, and forming trends with negative slopes, indicating the presence of a trace Os-Ir-rich phase that accumulated near the bottom of the lava lake, in the least MgO-rich cumulate samples. By contrast, Ru continued to be compatible with the fractionating mineral assemblage; Ru exhibits strong positive correlation with Cr, reflecting the major role of chromite on the liquidus, in controlling Ru abundances in the lava lake (**Figs. 5**). Rhenium, Pt, and Pd are characterized by strongly incompatible behavior throughout the lava lake; the data for these HSE follow olivine control lines, indicating that olivine fractionation alone was responsible for the variations of these elements over the entire range of lava lake compositions (**Fig. 5**).

Tonalites of the Vodla Block analyzed have low HSE abundances, averaging 0.03 ppb Re, 0.005 ppb Os, 0.003 ppb Ir, 0.008 ppb Ru, 0.13 ppb Pt, and 0.05 ppb Pd; the samples are characterized by suprachondritic $(Os/Ir)_N = 1.4$ and moderately fractionated $(Pd/Ir)_N = 10$ (**Table 1**, **Fig. 4**).

4.3. Re-Os isotopic data

The Re-Os isotopic data for the komatiitic basalts and tonalites obtained in this study are presented in **Table 1**; the lava lake data are also plotted on the Re-Os isochron diagram in **Fig. 6**. Twenty eight samples, including five olivine and nine chromite separates, define an isochron with a slope corresponding to an ISOPLOT Model 3 (Ludwig, 2003) age of 2407±6 Ma and an initial $^{187}Os/^{188}Os$ = 0.11242±22 ($\gamma^{187}Os$ = +1.7±0.2, 2SE). This Re-Os age is consistent with the Sm-Nd isochron age for the lava lake of 2410±34 Ma (Puchtel *et al.*, 1997) and represents our best estimate for the age of the lava lake and the uppermost Vetreny Belt suite. The much more precise initial $\gamma^{187}Os$ = +1.7±0.2 obtained in this study is slightly higher than the initial $\gamma^{187}Os$ = +0.3±1.1 reported by Puchtel *et al.* (2001).

The tonalites of the Vodla Block are characterized by an average initial $^{187}Os/^{188}Os$, calculated at the time of komatiite emplacement (2407 Ma) of ca. 0.97 (average initial $\gamma^{187}Os$ = +777). Regression of the data using ISOPLOT yields a Model 2 (Ludwig, 2003) age of 3334±710 Ma; this age is consistent with the emplacement age of the tonalites of 3213±32 Ma (Chekulaev *et al.*, 2009). The average initial $\gamma^{187}Os$ calculated at the time of tonalite emplacement is +304±64 (2SE).

4.4. Pt-Os isotopic data

The high-precision Os isotopic data for chromite separates from the komatiitic basalts are presented in **Table 2** and plotted on a Pt-Os isochron diagram in **Fig. 7.** Data for nine chromite separates define a regression line with a slope corresponding to an age of 2258±620 Ma, which is consistent, within the uncertainty, with the emplacement age of the lavas. The average calculated initial $^{186}Os/^{188}Os$ is

0.1198329±3 (initial $\varepsilon^{186}Os$ = +0.03±0.02, 2SE). It is slightly higher than the chondritic reference of (Brandon *et al.*, 2006) at the time of lava emplacement, but is well within the range of chondritic variations.

4.5. W abundances and isotopic data

Tungsten abundances and isotopic compositions for the komatiitic basalts and tonalites are reported in **Table 3**; the W abundance data are plotted on a W *vs.* MgO diagram in **Fig. 2** and the W isotopic data are plotted in **Fig. 8**. The komatiitic basalts have W concentrations ranging between 33 and 38 ppb in the olivine cumulate zone and 62-69 ppb in the lower part of the spinifex zone, with the upper chilled margin samples containing on average ~62 ppb W. The tonalites have W contents ranging between 54 and 169 ppb, with an average value of 95 ppb.

Tungsten abundances in the komatiitic basalts show a broad negative correlation with MgO contents (**Fig. 2**). The limited scatter observed is likely due to minor mobility of W in the upper part of the lava lake, whereas the cumulate samples plot as a compact group with a narrow range of W abundances.

The komatiitic basalts show resolvable positive ^{182}W anomalies, relative to the terrestrial standard (**Table 3**); the calculated average $\mu^{182}W$ value for the lava lake (defined as parts per million (ppm) deviation of the $^{182}W/^{184}W$ ratio of a given sample relative to the terrestrial reference standard) is +7.1±4.5 ppm (*N* = 12, 2SD).

The Vodla Block tonalites analyzed in this study also show positive ^{182}W anomalies (**Table 3**); these are nearly two times larger than those observed in the komatiitic basalts and average +12.6±4.5 ppm (*N* = 4, 2SD, **Fig. 8**).

4.6. Sm-Nd isotopic data

The Sm-Nd isotopic data for the komatiitic basalts and tonalites, as well as for two digestions of the USGS SRM BCR-1, are presented in **Table 4** and plotted in **Fig. 9** as μ^{142}Nd, or parts per million (ppm) deviations of $^{142}Nd/^{144}Nd$ measured in the samples from the average $^{142}Nd/^{144}Nd$ obtained for the Nd standard AMES run during the course of the entire analytical campaign. The average μ^{142}Nd value for the five komatiitic basalt samples analyzed is +0.5±2.8 ppm (2SD), and for the eight tonalite samples analyzed (including replicates), -0.4±5.2 ppm (2SD). For comparison, the average μ^{142}Nd for three separate digestions of the USGS SRM BCR-1 is +0.7±2.8 ppm (2SD). These μ^{142}Nd values are within the uncertainty of the average μ^{142}Nd value for the Nd standard AMES obtained during the course of this analytical campaign (**Fig. 9**).

The calculated initial ε^{143}Nd values for the komatiitic basalt samples analyzed in this study average −0.82±0.15 (2SE), which is identical to the average initial $\varepsilon^{143}Nd = -0.94\pm0.12$ (2SE) obtained for whole-rock komatiitic basalt samples and olivine and pyroxene separates by Puchtel *et al.* (1996). Regression of the data combined from the two studies yields an isochron age of 2403±32 Ma (MSWD = 0.90) and an average initial $\varepsilon^{143}Nd = -0.90\pm0.09$ (2SE).

The initial ε^{143}Nd values for the tonalite samples calculated at the time of tonalite emplacement (3213 Ma) range between +0.93 and +2.3, averaging +1.8±0.6 (2SE). This positive initial ε^{143}Nd value indicates derivation from a source with a time-integrated, slightly suprachondritic Sm/Nd ratio. The calculated T_{DM} Nd model ages range between 3.26 and 3.36 Ga, with an average age of 3292±47 Ma (2SE), identical to the average T_{DM} Nd model age of 3288±94 obtained by Kulikov *et al.* (1990) on a larger set of tonalite samples from the Vodla Block.

4.7. Lu-Hf isotopic data

The Lu-Hf isotopic data and Lu and Hf abundances for the komatiitic basalts and tonalites are listed in **Table 5**; the lava lake data are also plotted on a Lu-Hf isochron diagram in **Fig. 10**. The data for five whole-rock olivine cumulates and six pyroxene separates define an isochron with a slope corresponding to an age of 2451±79 Ma and an initial $^{176}Hf/^{177}Hf = 0.281230±40$ (initial $\varepsilon^{176}Hf = +0.65±1.4$). The average initial $^{176}Hf/^{177}Hf$, calculated as a mean of the initial $^{176}Hf/^{177}Hf$ ratios for the individual samples, using the emplacement age of 2407 Ma derived from the Re-Os isochron, and the measured $^{176}Hf/^{177}Hf$ and $^{176}Lu/^{177}Hf$ for each individual sample (**Table 5**), is 0.281252±6 (2SE), which translates into an initial $\varepsilon^{176}Hf = +0.4±0.2$.

The initial $\varepsilon^{176}Hf$ values for the tonalites calculated at the time of tonalite emplacement (3213 Ma) range between +1.1 and +4.8, averaging +2.5±1.6. Similarly to the tonalite Sm-Nd isotopic data, this positive initial $\varepsilon^{176}Hf$ value indicates derivation from a source with a time-integrated suprachondritic Lu/Hf ratio.

5. Discussion

5.1. Nd-Hf isotope and trace element systematics of the Vetreny lavas

Using the Sm-Nd isotope and lithophile trace element data for variably crustally contaminated komatiitic lavas collected from different stratigraphic levels within the Vetreny Belt, Puchtel *et al.* (1997) concluded that the Victoria's lava lake was ultimately derived from a komatiitic magma that was modified via ~50% fractional crystallization and 7-8% contamination with crustal rocks of the Vodla Block. However, both Hf isotopic and abundance data were not available at the time of that study. Here, we use the new lithophile trace element and Hf-Nd isotope data for both the Vodla Block tonalites and

528 the Victoria's lava lake komatiitic basalts, to better model the assimilation-fractional crystallization
529 (AFC) processes involved in the generation of the lava lake, as well as to estimate the initial Nd and Hf
530 isotopic compositions of the original komatiitic magma, prior to contamination. The MgO content of the
531 original Vetreny komatiite magma is assumed to be typical of late Archean komatiite magmas
532 worldwide, *i.e.,* ca. 27 wt.% (Bickle, 1982; Nisbet *et al.*, 1993; Arndt *et al.*, 2008).

533 One way to constrain the effects of AFC processes on a komatiitic system is by examination of the
534 magnitude of Eu anomalies. Both Bulk Continental Crust and Archean Continental Crust estimates show
535 negative Eu anomalies of 0.885 and 0.896, respectively (Rudnick and Fountain, 1995; Rudnick and Gao,
536 2014), whereas primary komatiitic lavas cannot have primary Eu anomalies due to the absence of
537 plagioclase in their sources, or plagioclase involvement in any subsequent crystal-liquid fractionation
538 prior to emplacement. For this study, the existing (Puchtel *et al.*, 1997) and the new Eu/Eu* (where Eu*
539 = $0.3258\times\sqrt{(Sm\times Gd)}$ is the abundance of Eu calculated for a chondrite-normalized REE pattern without
540 anomaly by interpolation of the abundances from Sm and Gd) and Sm-Nd isotopic data for Vetreny Belt
541 lavas were compiled. Further, ISOPLOT regression analysis of Eu/Eu* *versus* initial $\varepsilon^{143}Nd$, projected to
542 a Eu/Eu* = 1.0 (*i.e.*, no Eu-anomaly), was used to obtain an initial $\varepsilon^{143}Nd$ of +3.7±0.3 for the
543 uncontaminated, original Vetreny komatiitic magma (**Fig. 11**). We then used the calculated initial Nd
544 isotopic composition and Nd abundance of the original Vetreny komatiite magma, and the Nd isotopic
545 composition and Nd abundance of the crustal contaminant, calculated at the time of Victoria's lava lake
546 emplacement, to estimate the degree of crustal contamination of the Victoria's lava lake komatiitic
547 basalts. Further, using this degree of crustal contamination and the Hf isotopic compositions of the
548 contaminated Victoria's lava lake lava and the crustal contaminant, we calculated the initial Hf isotopic
549 composition of the original Vetreny komatiite magma.

550 The parameters used in the calculations are presented in **Table 6**. The Nd and Hf abundances of the
551 original Vetreny komatiite magma at 27 wt.% MgO were assumed to be similar to those of the emplaced
552 komatiite lavas from Alexo and Munro Township, Abitibi greenstone belt, Canada. These lavas were
553 estimated to contain ~27 wt.% MgO (Puchtel *et al.*, 2004b), and were also characterized by a degree of
554 LREE-depletion similar to that estimated for the original Vetreny komatiite magma ($(La/Sm)_N$ =
555 0.41±0.07 and 0.42±0.02 in the Vetreny and Abitibi lavas, respectively) on the basis of the $(La/Sm)_N$ *vs.*
556 $\varepsilon^{143}Nd(T)$ ISOPLOT regression (**Fig. 11**). These Nd and Hf abundances were compiled from the studies
557 of Blichert-Toft and Arndt (1999) and Puchtel *et al.* (2004b, 2009b) to be 1.44 and 0.420 ppm,
558 respectively. The Nd and Hf abundances in the crustal contaminant used were the average Nd and Hf
559 abundances obtained for the Vodla Block tonalites in this study (18.4±4.7 and 4.0±0.7 ppm,
560 respectively). The initial $\varepsilon^{143}Nd$ and $\varepsilon^{176}Hf$ values of the Vodla Block tonalites at the time of Vetreny
561 lava emplacement were calculated to have been −9.5±0.6 and −14.4±1.6, respectively (2SE), using their
562 measured, present-day Nd and Hf isotope compositions and Sm/Nd and Lu/Hf ratios. The Nd and Hf
563 isotope compositions of the contaminated Victoria's lava lake lava used were those compiled from this
564 study and the study of Puchtel *et al.* (1996).

565 The modeling results are presented in **Table 6**. The degree of crustal contamination estimated from
566 the mixing calculations is 4.0±0.4%. Using this degree of crustal contamination, the initial $\varepsilon^{176}Hf$ value
567 of the original Vetreny komatiite magma is calculated to be +6.3±0.5. As is evident from **Fig. 12**, the
568 data for the original, uncontaminated Vetreny komatiite magma plot on the terrestrial Sm/Nd *vs.* Lu/Hf
569 evolution curve (terrestrial array), together with the late Archean Kostomuksha, Belingwe, and Abitibi
570 komatiite systems. This suggests coupled behavior of the two isotopic systems in the mantle source of
571 the Vetreny komatiite magma, consistent with the similar behavior of the parent and daughter isotopes
572 of both isotope systems during upper mantle differentiation and crust-forming processes. Further, the

573 average μ^{142}Nd value of +0.5±2.8 obtained for the lava lake is also unremarkable, and suggests that no
574 significant deviation of the Sm/Nd ratio of the komatiite source from the dominant mantle occurred
575 during early Earth history.

576 In order to investigate the origin of the tonalites, we modeled their lithophile trace element
577 compositions. Based on their highly fractionated, heavy REE-depleted patterns, Archean tonalites are
578 generally considered to be derived from hydrous melting of a mafic crustal source, either through partial
579 melting of amphibolite, garnet amphibolite, or eclogite, in which hornblende and/or garnet are residual
580 phases, or by hornblende-controlled fractionation of hydrous basaltic magmas (Rapp *et al.*, 1991). In the
581 case of the Vodla Block tonalites, their derivation from a mafic precursor is supported by their positive
582 initial ε^{143}Nd and ε^{176}Hf values, consistent with Nd and Hf isotopic data for TTG gneisses worldwide
583 (e.g., Guitreau *et al.*, 2012).

584 Here, we model the REE composition of the putative mafic crust that the tonalitic melts were
585 derived from, using an equilibrium partial melting model and partition coefficients from Irving and Frey
586 (1978), Fujimaki *et al.* (1984), Bacon and Druitt (1988), and Sisson (1994). The results of the modeling
587 are presented in **Fig. 13**. The most HREE-depleted tonalite (sample K04), with the highest ε^{143}Nd value,
588 is calculated to be derived from melting of a rock with a basaltic composition with essentially
589 unfractionated HREE and slightly LREE-depleted patterns, in equilibrium with a Rut-Hbl-Gar-Cpx
590 mineral assemblage, at pressures between 12 and 20 Kb (Moyen and Martin, 2012). The most HREE-
591 enriched tonalite (sample K14), with the lowest ε^{143}Nd value, is calculated to be derived from melting of
592 a basaltic composition with slightly LREE-enriched and HREE-depleted patterns (**Fig. 13)**, in
593 equilibrium with a Mgt-Pl-Hbl-Cpx residual mineral assemblage, at pressures of ~10 Kb (Moyen and
594 Martin, 2012). These calculated mafic crust compositions are similar to those of two 3.5 Ga tholeiitic
595 basaltic sequences of the Warrawoona Group of the east Pilbara Craton in Western Australia (Green *et*

596 *al.*, 2000; Kato and Nakamura, 2003). Tholeiites of the Warrawoona Group may, therefore, represent
597 good proxies for the putative mafic crust that served as a precursor for the Vodla Block tonalites.
598 The average calculated time-integrated Sm/Nd and Lu/Hf ratios for the source of the Vodla Block
599 tonalites, within the uncertainties, also plot on the terrestrial array (**Fig. 12**). This indicates that, since the
600 initial Nd and Hf isotopic compositions of the tonalites reflect time-integrated Sm/Nd and Lu/Hf of their
601 respective precursors, the parental magmas to the tholeiitic sequences originated from mantle domains
602 that were characterized by Hf-Nd relationships similar to those habitually observed for upper mantle
603 rocks. In addition, the average μ^{142}Nd value of -0.4±5.2 for the tonalities is indistinguishable from the
604 terrestrial standard and permits only very limited fractionation of the Sm/Nd ratio by very early
605 differentiation processes in the sources of these rocks.

606 **5.2. HSE systematics of the Vetreny komatiite mantle source**

607 The Re-Os and Pt-Os isotopic systems provide insights into certain processes to which the more
608 traditional, lithophile element-based isotopic systems are less sensitive, including planetary accretion
609 and mantle and core differentiation. Here, we use the initial $^{186}Os/^{188}Os$ and $^{187}Os/^{188}Os$ ratios obtained
610 for the Vetreny komatiite system as a measure of the long-term evolution of Pt/Os and Re/Os in its
611 mantle source. In order to constrain the long-term source characteristics, we calculate the
612 parent/daughter elemental ratios necessary to arrive at the Os isotopic composition at the time of lava
613 lake formation by assuming generation of this mantle domain soon after Solar System formation.
614 However, because the original komatiite magma parental to the lava lake underwent AFC processes that
615 may have modified its Os isotopic composition, the effects of the AFC processes on Os must first be
616 evaluated. Here, we use the estimated degree of contamination (4.0%) and the Os isotopic and HSE
617 abundance data for the lava lake and the Vodla Block tonalites obtained, to estimate the effects of crustal

618 contamination on the initial $^{186}Os/^{188}Os$ and $^{187}Os/^{188}Os$ ratios, and to calculate the initial Os isotopic
619 composition of the source of the original Vetreny komatiite magma.

620 The parameters used in the modeling are presented in **Table 7**. For Re, Pt, and Os abundances of the
621 crustal end member, we used two model compositions, one being the average composition of the Vodla
622 Block tonalites (VBT) from this study and the other being composition of the upper continental crust
623 (UCC) from Peucker-Ehrenbrink and Jahn (2001). As mentioned earlier, the UCC in this part of the
624 Karelian granite-greenstone terrain consists of Vodla Block TTG gneisses with a U-Pb zircon age of
625 ~3.21 Ga (Lobach-Zhuchenko *et al.*, 1993; Chekulaev *et al.*, 2009). Assuming that the UCC in the area
626 was derived from a source with an average BSE $^{186}Os/^{188}Os = 0.1198304$ and $^{187}Os/^{188}Os = 0.10492$ at
627 3.21 Ga, it had ~800 Ma to evolve from this Os isotopic composition, with its respective Pt/Os and
628 Re/Os ratios, prior to being assimilated by the original Vetreny komatiite magma. For an estimate of the
629 Os abundance in the original komatiite magma that gave rise to the Vetreny lavas, an average Os
630 abundance of 1.92 ppb in late Archean komatiite lavas compiled from the studies of Puchtel and
631 Humayun (2005) and Puchtel *et al.* (2007, 2009b) was used.

632 The modeling shows that addition of 4.0% continental crustal material that had aged for 800 Ma, to
633 the original Vetreny komatiite magma will increase its initial $^{186}Os/^{188}Os$ and $^{187}Os/^{188}Os$ by either
634 0.0003 $\varepsilon^{186}Os$ and 0.03 $\gamma^{187}Os$ units when the VBT crustal endmember is used, or 0.001 $\varepsilon^{186}Os$ and 0.4
635 $\gamma^{187}Os$ units when the UCC crustal end member is used.

636 For the initial $^{186}Os/^{188}Os$, this shift is beyond the current level of isotopic resolution, irrespective of
637 which crustal contaminant end member is used. Therefore, the obtained initial $^{186}Os/^{188}Os =$
638 0.1198329 ± 3 ($\varepsilon^{186}Os(T) = +0.03\pm0.02$) for the lava lake is concluded to closely approximate that in the
639 source of the original Vetreny komatiite magma. Using the early Solar System initial $^{186}Os/^{188}Os =$

640 0.1198269 at 4567 Ma (Brandon *et al.*, 2006), it is calculated that this source would have evolved to its
641 $^{186}Os/^{188}Os$ = 0.1198329 at 2407 Ma with a time-integrated $^{190}Pt/^{188}Os$ = 0.00187±6.

642 The initial $^{187}Os/^{188}Os$ in the source of the original Vetreny komatiite lava corrected for the crustal
643 contribution is calculated to be either 0.11236±21 ($\gamma^{187}Os(T)$ = +1.6±0.2) or 0.11199±21 ($\gamma^{187}Os(T)$ =
644 +1.3±0.2), depending on whether VBT or UCC crustal end members are used, respectively. The very
645 low average Re abundances measured in the Vodla Block tonalites likely indicate Re loss in these rocks
646 during alteration and/or metamorphism. As such, we use the UCC composition of Peucker-Ehrenbrink
647 and Jahn (2001) as an estimate of the Re content in the crustal contaminant to calculate that the Vetreny
648 komatiite mantle source would have evolved from an early Solar System initial $^{187}Os/^{188}Os$ = 0.09531 at
649 4558 Ma (Smoliar *et al.*, 1996) to its initial $^{187}Os/^{188}Os$ = 0.11199±21 at 2407 Ma with a time-integrated
650 $^{187}Re/^{188}Os$ = 0.439±6.

651 These time-integrated $^{187}Re/^{188}Os$ and $^{190}Pt/^{188}Os$ ratios in the source of the Vetreny komatiite
652 magma are within the range of those observed for chondritic meteorites (**Fig. 14**; average $^{187}Re/^{188}Os$ =
653 0.410±0.051 (2SD), as compiled from the data of Walker *et al.* (2002), Brandon *et al.* (2005), and
654 Fischer-Gödde *et al.* (2010), and average $^{190}Pt/^{188}Os$ = 0.00180±17 (2SD), as compiled from the data of
655 Horan *et al.* (2003), Brandon *et al.* (2005, 2006), Fischer-Gödde *et al.* (2010), and van Acken *et al.*
656 (2011). These values represent our best estimates of the relative Re, Pt, and Os abundances in the mantle
657 source of the original Vetreny komatiite magma.

658 The calculated initial Os isotope ratios in the source of the Vetreny komatiite system, as was also the
659 case with the initial Nd and Hf isotope ratios, are unremarkable. A compilation of high-precision
660 $^{187}Os/^{188}Os$ isotopic data for Archean komatiites indicates that most sources of Archean komatiite
661 systems were characterized by initial $\gamma^{187}Os$ values ranging from −0.1 to +1.3, well within the range of
662 90% of chondritic meteorites (**Fig. 14a**). The only exceptions to this are the 3.55 Ga Schapenburg and

2.82 Ga Kostomuksha komatiites (Puchtel *et al.*, 2005, 2009a). The limited data set available for $^{186}Os/^{188}Os$ isotope systematics of komatiites indicates somewhat greater variability outside the chondritic range compared to $^{187}Os/^{188}Os$. The initial $^{186}Os/^{188}Os$ ratios that have been generated to date indicate that mantle sources of three late Archean komatiite systems (Abitibi, Belingwe, and Vetreny) evolved with time-integrated Pt/Os within the chondritic range (**Fig. 14b**). The high initial $^{186,187}Os/^{188}Os$ ratios of the mantle source of the 2.8 Ga Kostomuksha komatiites, however, require long-term suprachondritic Pt/Os and Re/Os (Puchtel *et al.*, 2005). By contrast, the early Archean komatiite systems evolved with fractionated (non-chondritic) time-integrated Pt/Os ratios, but were characterized by essentially chondritic Re/Os, thus displaying decoupling of the Re-Os and Pt-Os isotopic systems (Puchtel *et al.*, 2014).

More than 90% of the HSE budget of the mantle resides in two types of sulfides (Alard *et al.*, 2000; Lorand and Alard, 2001; Luguet *et al.*, 2007). The high-temperature Os-Ir-Ru-Rh-rich Fe-Ni monosulfide solid solution (*mss*) forms rounded inclusions in olivine, whereas low-temperature, irregular-shaped Cu-Ni sulfides occupy intergranular space. During partial melting of mantle peridotite, Cu-Ni sulfides enter the melt, whereas the mss remains trapped in the melting residue until the degree of melting reaches ~25% (Barnes *et al.*, 1985; Keays, 1995), at which point all the sulfide in the residue gets consumed and, as the degree of melting continues to increase, the magma becomes sulfide-undersaturated. It has also recently been shown that decrease in fS_2 with increase in degree of melting triggers exsolution of Os-Ir alloys from the refractory mss in the residue (Fonseca *et al.*, 2011, 2012). All low-degree (basalts) and the majority of higher-degree (picrites and komatiites) partial melts are charactrized by compatible behavior of Os and Ir during magmatic differentiation, indicating that their parental magmas remained saturated in Os-Ir alloys (Puchtel *et al.*, 2004b; Barnes and Fiorentini, 2008). However, some lavas, such as the 2.8 Ga Kostomuksha komatiites and the 3.55 Ga Schapenburg

686 komatiites, exhibit incompatible behavior of these HSE during magma differentiation, likely indicating
687 complete exhaustion of Os-Ir alloys in the mantle sources of these komatiites (Puchtel and Humayun,
688 2005; Puchtel *et al.*, 2009a).

689 In order to calculate the absolute HSE abundances in the mantle source of the original Vetreny
690 komatiite magma, the projection technique of Puchtel *et al.* (2004b) is used here, with some additional
691 assumptions. As has been discussed by these authors, one of the pre-requisites for this protocol to be
692 applicable for calculating the HSE composition of the mantle source of a komatiite lava from its HSE
693 abundances is the complete exhaustion of sulfides harboring Pd, Pt, and part of the Re in the mantle
694 source, during partial melting. The original Vetreny komatiite magma is estimated to have formed via
695 >35% partial melting based on its calculated incompatible lithophile trace element abundances. As such,
696 it was most likely sulfide undersaturated prior to emplacement, and maintained this status through the
697 AFC processes. The strongest evidence for the sulfide-undersaturated nature of the emplaced Vetreny
698 komatiitic basalt lava is provided by the behavior of Pd and the chalcophile element Cu during
699 differentiation of the lava lake. The Cu and Pd abundances measured in samples collected from across
700 the lava lake plot on the olivine control lines in the MgO vs. Cu (**Fig. 2**) and MgO vs. Pd (**Fig. 5**)
701 variation diagrams, indicating that sulfide liquid was not a fractionating phase over the entire range of
702 the lava lake compositions. We conclude, therefore, that this requirement was met for the Vetreny
703 komatiite system.

704 Although lavas of the Victoria's lava lake are remarkably fresh, and all HSE were shown to be
705 unaffected by alteration, due to the complex differentiation history of the original Vetreny komatiite
706 magma prior to emplacement, only abundances of the incompatible elements Pt and Pd in its source can
707 be estimated with a sufficiently high degree of accuracy.

The first step in this procedure is to establish the original komatiite liquid lines of descent. For the incompatible Pt and Pd, the original komatiite liquid lines of descent should pass through the composition of the olivine that was in equilibrium with the original komatiite magma and the composition of the Victoria's lava lake emplaced komatiitic basalt lava. The results of these calculations are presented in **Table 7**. Since the lava lake olivines analyzed in this study crystallized from the evolved komatiitic basalt liquid containing ~15% MgO, and since we are interested in the HSE content of the original komatiite magma, the HSE abundance data for the Pyke Hill olivine from Puchtel *et al.* (2009b) were used instead. This choice was also based on the similarity of the MgO contents of the original komatiite magmas at both localities. Besides, since both Pt and Pd are highly incompatible in olivine (e.g., Brenan *et al.*, 2003), small variations in the abundances of these elements in olivine have very limited effect on the regression calculations, the most important parameter being the MgO content of the olivine. The abundances of Pt and Pd are calculated to be 8.6±0.9 and 8.4±0.9 ppb in the original Vetreny komatiite magma and 4.9±0.5 and 4.8±0.5 ppb in its mantle source.

The calculated total concentrations of Pt and Pd in the source of the Vetreny komatiite system are plotted as a function of age and compared with those in the sources of Archean komatiite systems and in the estimate for the modern BSE (**Fig. 15**). In the calculations of the Pt+Pd totals, the relative weight of the Pd contribution was normalized to that of Pt on the basis of their relative abundances in an average CI chondrite Orgueil (Horan et al., 2003). In order to do that, the abundance of Pd, which is lower in Orgueil by a factor of 1.52, was multiplied by 1.52 and added to that of Pt. The total Pt and Pd abundances in the Vetreny komatiite system are calculated to be 66±7% of those present in the estimates for the modern BSE of Becker *et al.* (2006).

As is evident from **Fig. 15**, the total Pt and Pd abundances in the sources of late Archean komatiite systems span a substantial range, from 58±7% in the 2.69 Ga Belingwe system to 85±5% in the 2.72 Ga

731 Abitibi system, of the total Pt and Pd present in the estimates for the modern BSE, with the Vetreny
732 komatiite system at 66±7% being at the lower end of this range. Within the uncertainties, the total Pt and
733 Pd abundances in some of the late Archean komatiite systems, e.g., Abitibi and Kostomuksha, overlap
734 with those in the estimates for the BSE, whereas others (Vetreny, Belingwe, and Volotsk-
735 Kamennoozero) fall slightly (by 14-20%, when the full uncertainties on the estimates are considered)
736 short of reaching that level. Further, the total Pt and Pd abundances in the sources of two out of three
737 early Archean komatiite systems are within the range of those in their late Archean counterparts, varying
738 from 56±12% for Komati to 65±10% for Weltevreden, of the total Pt and Pd present in the estimates for
739 the modern BSE, whereas the third early Archean komatiite system (the 3.55 Ga Schapenburg) is
740 characterized by much lower Pt and Pd abundances (27±4%: Puchtel *et al.*, 2009a).

741 The observations that the HSE occur in roughly chondritic relative proportions in the upper mantle,
742 and that absolute HSE abundances are two- to four orders of magnitude higher than might be expected
743 based on low-pressure metal-silicate experimental partitioning data (Kimura *et al.*, 1974), have led to the
744 concept of late accretion (Chou *et al.*, 1983; Morgan, 1985). Issues related to late accretion are highly
745 debated, including the time frame within which the late accreted material was delivered to Earth and
746 homogenized within the mantle, as well as the composition of the late accreted material itself. Some of
747 the uncertainties stem from the fact that HSE abundances in the Archean mantle are not well
748 constrained, and the causes of these apparent variations in HSE abundances in the early Earth's mantle
749 are not well understood. For example, on the basis of studies of 3.81 Ga peridotites from West
750 Greenland and 3.46 Ga komatiites from Western Australia, Bennett *et al.* (2002) concluded that any
751 HSE-rich components added to the mantle via late accretion must have been transported into and
752 become broadly homogenized within the mantle by 3.8 Ga. In contrast to these conclusions, Maier *et al.*
753 (2009), on the basis of their studies of Pt and Pd contents in komatiitic lavas of various ages, argued for

754 a gradual increase in the HSE abundances in the terrestrial mantle from ~3.5 to ~2.9 Ga due to the slow
755 downward mixing of a "late veneer" of chondritic impactors. Our present results, considered together
756 with the data for the early and late Archean komatiite systems compiled from Puchtel and Humayun
757 (2001, 2005) and Puchtel *et al.* (2004a, 2004b, 2005, 2007, 2009a,b, 2014), show no evidence of the
758 putative trend of increasing HSE abundances in komatiitic sources from 3.5 to 2.7 Ga. Our results also
759 indicate that, in some cases, variations in the HSE abundances between late Archean komatiite systems
760 were even greater than between the late and early Archean komatiite systems (**Fig. 15**). As also
761 concluded by Puchtel *et al.* (2014), rather than downward mixing of an HSE-rich late veneer, the HSE
762 concentration variations observed in early and late Archean komatiite systems may reflect sluggish
763 mixing of diverse post-magma ocean domains characterized by variably-fractionated lithophile and
764 siderophile element abundances. However, we also find that at least some early Archean komatiite
765 systems (*e.g.*, 3.55 Ga Schapenburg with only 27±4% of the total Pt and Pd abundance estimates for the
766 modern BSE) were derived from mantle sources strongly depleted in HSE.

767 **5.3. Tungsten abundances and isotopic composition of the Vetreny komatiite mantle source**

768 Under the relatively oxidizing conditions of the modern terrestrial mantle, W behaves as a highly
769 incompatible lithophile trace element, with a degree of incompatibility that is broadly similar to that of
770 U (Arevalo and McDonough, 2008; König *et al.*, 2011). The late Archean mantle was most likely
771 characterized by an oxidation state similar to that of the modern mantle, as indicated by partitioning
772 studies of redox-sensitive elements, such as Fe, V, and Cr (Canil, 1997; Delano, 2001; Li and Lee, 2004;
773 Berry *et al.*, 2008). As a result, during melting of the late Archean mantle, W was likely characterized
774 by a degree of incompatibility similar to that of the present day; this is also suggested by its negative
775 correlation with indices of magmatic differentiation (**Fig. 2**). Therefore, the W abundance in the source
776 of the Vetreny komatiite system can be calculated in the same manner as the incompatible HSE, using

777 the projection technique outlined above, except that, due to much higher W concentrations in continental
778 crustal rocks compared to komatiitic magmas, the AFC effects on the W abundances and W isotopic
779 composition of the original Vetreny komatiite magma must be evaluated and accounted for.
780 In order to do that, we must first remove the effects of fractional crystallization on the W
781 concentration in the contaminated Vetreny komatiite magma; this gives a W abundance for the komatiite
782 magma with 27 wt.% MgO, post-crustal contamination. The W content of the olivine in equilibrium
783 with the primary Vetreny komatiite magma can be calculated iteratively using the calculated W content
784 of the Vetreny komatiite magma with 27 wt.% MgO and an olivine-liquid partition coefficient of U as a
785 proxy for that of W, $D_U^{ol\text{-}liq} = 2\times10^{-5}$ (Kennedy *et al.*, 1993). The calculations yield a W content of
786 39.3±1.7 ppb. This estimate is then used to remove the effects of crustal contamination.
787 The measured average W abundance in the Vodla Block tonalites is 95 ppb; this is a factor of ~20
788 lower than in the estimates for the UCC or BCC of Rudnick and Gao (2014). Since W is a fluid-mobile
789 element, its low concentration in the Vodla Block tonalites, similarly to Re, is likely the result of loss
790 during alteration and/or metamorphism of the rocks. Another fluid-mobile element is U. The average U
791 abundance in the Vodla Block tonalites is 0.268 ppm, which again is a factor of 5 to10 lower than in the
792 estimates for the UCC, BCC, or Archean CC (Rudnick and Founrain, 1995; Rudnick and Gao, 2014). In
793 order to correct for the loss of W during alteration, we use the average concentration of the fluid-
794 immobile element Th = 3.51 ppm in the Vodla Block tonalites to calculate the true abundance of W =
795 0.635 ppm using the W/Th ratio of the UCC and BCC of 0.18 (Rudnick and Gao, 2014). Using this
796 estimate for the W abundance in the crustal contaminant and the calculated degree of crustal
797 contamination of 4.0%, the W abundance in the original Vetreny komatiite magma and its mantle source
798 are calculated to be 14.5±1.8 ppb and 8.1±0.9 ppb, respectively. This estimate of the W abundance in

the source of the Vetreny komatiite system is identical to that of the modern mantle estimate of 8.3±7.1 ppb (Arevalo and McDonough, 2008).

The calculated W abundance of 14.5±1.8 ppb in the original Vetreny komatiite magma can then be used to evaluate the effect of crustal contamination on its W isotopic composition using the average W isotopic composition of the Vodla Block tonalites ($\mu^{182}W$ = +12.6±4.5) and their W concentration of 0.635 ppm. Our calculations indicate that the permissible range of $\mu^{182}W$ values for the original Vetreny komatiite magma is −0.5±4.5 (2SD), when the measurement uncertainties are taken into account. This value is indistinguishable from the value for the modern terrestrial standard of 0.0±4.5 ppm (2SD).

The diagram of W isotopic compositions *versus* calculated HSE abundances in the mantle sources of Archean komatiites studied so far (**Fig. 16)** illustrates the effects of addition of late accreted chondritic material on the W isotopic composition of the BSE, with the assumption that the entire HSE budget of the modern BSE was established as a result of late accretion. The $\mu^{182}W$ of BSE prior to late accretion is constrained by the recent $^{182}W/^{184}W$ data for the lunar mantle to be +21±5 ppm (Touboul *et al.*, 2015), with the uncertainty on pre-late accretion BSE W isotopic composition defined by the uncertainty on the W isotopic composition of the lunar mantle. Accordingly, the W isotopic composition of the primordial BSE containing very low HSE, due to efficient core formation, would have evolved toward the present-day BSE W isotopic composition as more chondritic material was added during late accretion. In this model, the source of the Vetreny komatiite system plots, although barely, within the field of mantle compositions established by late accretion (**Fig. 16)**, indicating that the W isotopic composition and HSE systematics of the Vetreny komatiite system most likely was established as a result of late accretion of chondritic material to Earth.

It is also possible that the $^{182}W/^{184}W$ isotopic composition of the mantle has not been well homogenized after core formation was complete. Consequently, the source of the Vetreny komatiites

may have started with a slightly lower $\mu^{182}W$ than the ambient mantle, prior to late accretion, and also had a smaller amount of late accreted material added to it. The lesser proportion of late accretion brought the $\mu^{182}W$ of the Vetreny komatiite source down less than that of the ambient mantle, but it ended up close to zero because of the lower $\mu^{182}W$ starting point (**Fig. 16**). Due to the rather large uncertainty on the W isotopic composition of the Vetreny komatiite system, it is at present not possible to distinguish between these two scenarios.

Owing to their complex magmatic history, it is not straightforward to interpret the observed W isotopic composition of the Vodla Block tonalites. We argued in the previous sections that the Vodla Block tonalites were derived from melting of a mafic precursor, most likely hydrated early Archean mafic crust. This crust either preserved a W isotopic signature of a mantle differentiation event that occurred within the first 50 Ma of Solar System history, while ^{182}Hf was still extant, or it contains a fraction of a primordial mantle component that has received only between 0 and 60% of late accreted component compared to the BSE of today. The second scenario appears to be more plausible, given the lack of a ^{142}Nd anomaly in these rocks; however, to confirm or reject this hypothesis, an estimate of HSE abundances in the source of the hypothetical mafic crust is required, which, due to poorly constrained partitioning behavior of HSE during formation of tonalitic magmas, at present is impossible to obtain with any reasonable degree of accuracy.

Plotted in **Fig. 8** are published ^{182}W data for Archean rocks. The reported ^{182}W anomalies vary from 0 to +25 ppm for the early and late Archean geological record. The hypotheses that have been put forward to explain these anomalies include metal-silicate and silicate-silicate differentiation during the lifetime of ^{182}Hf (Touboul *et al.*, 2012) and/or derivation from mantle that was isolated from a HSE-rich and ^{182}W-depleted late accretionary component (Willbold *et al.*, 2011, 2015; Touboul *et al.*, 2014; Rizo

et al., 2016). This study presents data for 3.2 Ga rocks that show an $^{182}W/^{184}W$ isotopic anomaly of +13 ppm, similar in magnitude to both 3.85 Ga Isua and 2.82 Ga Kostomuksha rocks.

Very few rocks younger than 3.5 Ga have $^{142}Nd/^{144}Nd$ ratios deviating from the terrestrial standard by more than 3 ppm (Debaille *et al.*, 2013; Rizo *et al.*, 2013), indicating that the magnitude of ^{142}Nd anomalies decreases over time, likely as a result of re-mixing of early depleted and early enriched mantle reservoirs. However, there does not seem to be any corresponding decrease in the magnitude of ^{182}W anomalies over time (**Fig. 8**). This may indicate decoupling of the two isotopic systems due to different processes responsible for the origin and re-homogenization of primordial heterogeneities in the mantle, such as delivery of the HSE via late accretion and crystal-liquid fractionation in a magma ocean, or re-mobilization of W via fluid-rock interaction (e.g., Rizo *et al.*, 2016).

6. Concluding remarks

Komatiites may be the best candidates in the surviving rock record for constraining the chemical composition of the early terrestrial mantle. Although some of them may have undergone fractional crystallization and were contaminated with material of the continental crust upon emplacement, important and unique information can be gleaned from komatiites once the veil of these processes is lifted. In this study, we report new Os isotope and HSE abundance data, in combination with Nd, Hf, and W isotope and abundance data, for 2.41 Ga komatiitic basalts from the Vetreny Belt and for 3.21 Ga tonalites of the adjacent Vodla Block in the Fennoscandian Shield.

The komatiitic basalts are shown to be derived from fractional crystallization of a strongly LREE-depleted komatiitic magma with ~27 wt.% MgO that assimilated ca. 4.0% of continental crustal material represented by the Vodla Block tonalites. Using the Os isotopic and HSE abundance data obtained for the tonalites, it is estimated that crustal contamination had only very minor effect on the Os isotopic composition of the original Vetreny komatiitic magma, with the calculated initial $\varepsilon^{186}Os$ and $\gamma^{187}Os$

867 values that are indistinguishable, within the respective uncertainties, from the chondritic reference
868 values; these values represent our best estimate of the time-integrated Re/Os and Pt/Os of the mantle at
869 the Archean-Proterozoic boundary.

870 Crustal contamination had markedly stronger effects on the Sm-Nd, Lu-Hf, and Hf-W isotopic
871 systems of the original Vetreny komatiite magma. When the effects of crustal contamination are
872 removed, the Vetreny komatiite source shows coupled behavior of the Nd-Hf isotope systematics,
873 plotting together with other late Archean komatiite systems on the Nd-Hf terrestrial array. The positive
874 ^{182}W anomaly of +7.1±4.5 ppm observed in the Victoria's lava lake is also shown to be derived from the
875 Vodla Block tonalites, which exhibit a larger ^{182}W anomaly of +12.6±4.5 ppm. The tonalites were
876 characterized by positive initial ε^{143}Nd and ε^{176}Hf, indicating their derivation from melting of a
877 precursor with time-integrated suprachondritic Sm/Nd and Lu/Hf, most likely ancient mafic crust, as
878 indicated by melting models based on REE abundances. This mafic crust must have recorded very early
879 differentiation processes that occurred within the first 50 Ma of Solar System history.

880 The absolute HSE abundances in the mantle source of the Vetreny komatiite system are calculated to
881 be 66±7% of those estimated for the present-day BSE. Coupled with the W isotopic composition of the
882 original komatiites corrected for crustal contamination (μ^{182}W = −0.5±4.5 ppm), these observations
883 indicate that the W-HSE systematics of the Vetreny komatiite system most likely were established as a
884 result of late accretion of chondritic material to Earth. Our present results, considered together with the
885 available high-quality data for other early and late Archean komatiite systems, show no trend of
886 increasing HSE abundances in komatiitic sources from 3.5 to 2.7 Ga; in some cases, variations in the
887 HSE abundances between individual late Archean komatiite systems are even greater than between late
888 and early Archean komatiite systems. These new data provide further support to the conclusion reached
889 by Puchtel *et al.* (2014) that rather than slow downward mixing of an HSE-rich late veneer throughout

890 the Archean, the HSE concentration variations observed in early and late Archean komatiite systems
891 may reflect sluggish mixing of diverse post-magma ocean domains characterized by variably-
892 fractionated lithophile and siderophile element abundances.
893

894 ## Acknowledgments

895 This work was supported by the NSF grants EAR-0946629 and EAR-1447174 to I.S. Puchtel, NSF-
896 CSEDI grants EAR1160728 and EAR1265169 to R.J. Walker, and ANR grant ANR-10-BLAN-0603
897 M&Ms to J. Blichert-Toft. These sources of support are gratefully acknowledged. We are indebted to
898 David van Acken and two anonymous experts for thorough reviews that helped improve the original
899 version of the manuscript. We thank V. Kevlich for mineral separation, Valentina Puchtel for help with
900 chemical preparation of samples, and Richard Ash for help with ICP-MS analyses.
901
902

References

Abouchami, W., Boher, M., Michard, A., and Albarède, F., 1990. A major 2.1 Ga event of mafic magmatism in West Africa: An early stage of crustal accretion. Journal of Geophysical Research **95**(B11): 17605-17629.

Aitken, B.G., and Echeverria, L.M., 1984. Petrology and geochemistry of komatiites and tholeiites from Gorgona Island, Colombia. Contributions to Mineralogy and Petrology **86**(1): 94-105.

Alapieti, T.T., Filen, B.A., Lahtinen, J.J., Lavrov, M.M., Smolkin, V.F., and Voitsekhovsky, S.N., 1990. Early Proterozoic layered intrusions in the northeastern part of the Fennoscandian Shield. Mineralogy and Petrology **42**: 1-22.

Alard, O., Griffin, W.L., Lorand, J.-P., Jackson, S.E., and O'Reilly, S.Y., 2000. Non-chondritic distribution of the highly siderophile elements in mantle sulfides. Nature **407**(6806): 891-894.

Amelin, Y.V., Heaman, L.M., and Semenov, V.S., 1995. U-Pb geochronology of layered mafic intrusions in the eastern Baltic Shield: implications for the timing and duration of Paleoproterozoic continental rifting. Precambrian Research **75**(1-2): 31-46.

Arevalo, R., and McDonough, W.F., 2008. Tungsten geochemistry and implications for understanding the Earth's interior. Earth and Planetary Science Letters **272**(3-4): 656-665.

Arndt, N.T., 1977. Thick, layered peridotite-gabbro lava flows in Munro Township, Ontario. Canadian Journal of Earth Sciences **14**(11): 2620-2637.

Arndt, N.T., Lesher, C.M., and Barnes, S.J. (2008). Komatiite. Cambridge, UK, Cambridge University Press.

Bacon, C.R., and Druitt, T.H., 1988. Compositional Evolution of the Zoned Calcalkaline Magma Chamber of Mount-Mazama, Crater Lake, Oregon. Contributions to Mineralogy and Petrology **98**(2): 224-256.

Balashov, Y.A., Bayanova, T.B., and Mitrofanov, F.P., 1993. Isotope data on the age and genesis of layered basic-ultrabasic intrusions in the Kola Peninsula and northern Karelia, northeastern Baltic Shield. Precambrian Research **64**(1-4): 197-205.

Barley, M.E., Pickard, A.L., and Sylvester, P.J., 1997. Emplacement of a large igneous province as a possible cause of banded iron formation 2.45 billion years ago. Nature **385**(6611): 55-58.

Barnes, S.-J., Naldrett, A.J., and Gorton, M.P., 1985. The origin of the fractionation of platinum-group elements in terrestrial magmas. Chemical Geology **53**(3-4): 303-323.

Barnes, S.J., and Fiorentini, M.L., 2008. Iridium, ruthenium and rhodium in komatiites: Evidence for iridium alloy saturation. Chemical Geology **257**(1-2): 44-58.

Becker, H., Horan, M.F., Walker, R.J., Gao, S., Lorand, J.-P., and Rudnick, R.L., 2006. Highly siderophile element composition of the Earth's primitive upper mantle: Constraints from new data on peridotite massifs and xenoliths. Geochimica et Cosmochimica Acta **70**(17): 4528-4550.

Begemann, F., Ludwig, K.R., Lugmair, G.W., Min., K., Nyquist, L.E., Patchett, P.J., Renne, P.R., Shih, C.-Y., Villa, I.M., and Walker, R.J., 2001. Call for an improved set of decay constants for geochronological use. Geochimica et Cosmochimica Acta **65**(1): 111-121.

Bennett, V.C., Nutman, A.P., and Esat, T.M., 2002. Constraints on mantle evolution from $^{187}Os/^{188}Os$ isotopic compositions of Archean ultramafic rocks from southern West Greenland (3.8 Ga) and Western Australia (3.46 Ga). Geochimica et Cosmochimica Acta **66**(14): 2615-2630.

Berry, A.J., Danyushevsky, L.V., O'Neill, H.S.C., Newville, M., and Sutton, S.R., 2008. Oxidation state of iron in komatiitic melt inclusions indicates hot Archaean mantle. Nature **455**(7215): 960-U42.

Bickle, M.J. (1982). The magnesium contents of komatiitic liqiuds. London, George Allen and Unwin.

947 Birck, J.L., Roy-Barman, M., and Capman, F., 1997. Re-Os isotopic measurements at the femtomole
948 level in natural samples. Geostandards Newsletter **20**(1): 19-27.
949 Blichert-Toft, J., 2001. On the Lu-Hf isotope geochemistry of silicate rocks. Geostandards Newsletter-
950 the Journal of Geostandards and Geoanalysis **25**(1): 41-56.
951 Blichert-Toft, J., and Albarède, F., 1997. The Lu-Hf isotope geochemistry of chondrites and the
952 evolution of the mantle-crust system. Earth and Planetary Science Letters **148**(1-2): 243-258.
953 Blichert-Toft, J., Albaréde, F., Rosing, M., Frei, R., and Bridgwater, D., 1999. The Nd and Hf isotopic
954 evolution of the mantle through the Archean. Results from the Isua supracrustals, West
955 Greenland, and from the Birimian terranes of West Africa. Geochimica et Cosmochimica Acta
956 **63**(22): 3901-3914.
957 Blichert-Toft, J., and Arndt, N.T., 1999. Hf isotope compositions of komatiites. Earth and Planetary
958 Science Letters **171**(3): 439-451.
959 Blichert-Toft, J., Boyet, M., Telouk, P., and Albarede, F., 2002. ^{147}Sm-^{143}Nd and ^{176}Lu-^{176}Hf in eucrites
960 and the differentiation of the HED parent body. Earth and Planetary Science Letters **204**(1-2):
961 167-181.
962 Blichert-Toft, J., Chauvel, C., and Albaréde, F., 1997. Separation of Hf and Lu for high-precision
963 isotope analysis of rock samples by magnetic sector multiple collector ICP-MS. Contributions to
964 Mineralogy and Petrology **127**(3): 248-260.
965 Blichert-Toft, J., and Puchtel, I.S., 2010. Depleted mantle sources through time: Evidence from Lu-Hf
966 and Sm-Nd isotope systematics of Archean komatiites. Earth and Planetary Science Letters
967 **297**(3-4): 598-606.
968 Bouvier, A., Vervoort, J.D., and Patchett, P.J., 2008. The Lu-Hf and Sm-Nd isotopic composition of
969 CHUR: Constraints from unequilibrated chondrites and implications for the bulk composition of
970 terrestrial planets. Earth and Planetary Science Letters **273**(1-2): 48-57.
971 Boyet, M., and Carlson, R.W., 2005. ^{142}Nd evidence for early (> 4.53 Ga) global differentiation of the
972 silicate Earth. Science **309**(5734): 576-581.
973 Brandon, A.D., Humayun, M., Puchtel, I.S., and Zolensky, M., 2005. Re-Os isotopic systematics and
974 platinum group element composition of the Tagish Lake carbonaceous chondrite. Geochimica et
975 Cosmochimica Acta **69**(6): 1619-1631.
976 Brandon, A.D., Walker, R.J., and Puchtel, I.S., 2006. Platinum-osmium isotope evolution of the Earth's
977 mantle: Constraints from chondrites and Os-rich alloys. Geochimica et Cosmochimica Acta
978 **70**(8): 2093-2103.
979 Brenan, J.M., McDonough, W.F., and Dalpé, C., 2003. Experimental constraints on the partitioning of
980 rhenium and some platinum-group elements between olivine and silicate melt. Earth and
981 Planetary Science Letters **212**(1-2): 135-150.
982 Brown, M., 2006. Duality of thermal regimes is the distinctive characteristic of plate tectonics since the
983 Neoarchean. Geology **34**(11): 961-964.
984 Campbell, I.H., and Griffiths, R.W., 1992. The changing nature of mantle hotspots through time:
985 Implications for the chemical evolution of the mantle. Journal of Geology **92**(5): 497-523.
986 Canil, D., 1997. Vanadium partitioning and the oxidation state of Archaean komatiite magmas. Nature
987 **389**(6653): 842-845.
988 Chase, C.G., and Patchett, P.J., 1988. Stored mafic/ultramafic crust and early Archaean mantle
989 differentiation. Earth and Planetary Science Letters **91**(1-2): 66-72.
990 Chekulaev, V.P., Arestova, N.A., Berezhnaya, N.G., and Presnyakov, S.L., 2009. New data on the age
991 of the oldest tonalite-trondhjemite association in the Baltic Shield. Stratigraphy and Geological
992 Correlation **17**(2): 230-234.

993 Chou, C.-L., Shaw, D.M., and Crocket, J.H., 1983. Siderophile trace elements in the Earth's oceanic
994 crust and upper mantle. Journal of Geophysical Research **88**(S2): A507-A518.
995 Ciborowski, T.J.R., Kerr, A.C., Ernst, R.E., McDonald, I., Minifie, M.J., Harlan, S.S., and Millar, I.L.,
996 2015. The Early Proterozoic Matachewan Large Igneous Province: Geochemistry, Petrogenesis,
997 and Implications for Earth Evolution. Journal of Petrology **56**(8): 1459-1494.
998 Coffin, M.F., and Eldholm, O., 1994. Large igneous provinces: crustal structure, dimensions and
999 external consequences. Reviews of Geophysics **32**(1): 1-36.
1000 Cohen, A.S., and Waters, F.G., 1996. Separation of osmium from geological materials by solvent
1001 extraction for analysis by thermal ionisation mass spectrometry. Analytica Chimica Acta **332**(2-
1002 3): 269-275.
1003 Condie, K.C., 1986. Origin and early growth rate of continents. Precambrian Research **32**(4): 261-278.
1004 Creaser, R.A., Papanastassiou, D.A., and Wasserburg, G.J., 1991. Negative Thermal Ion Mass-
1005 Spectrometry of Osmium, Rhenium, and Iridium. Geochimica et Cosmochimica Acta **55**(1): 397-
1006 401.
1007 Debaille, V., O'Neill, C., Brandon, A.D., Haenecour, P., Yin, Q.-Z., Mattielli, N., and Treiman, A.H.,
1008 2013. Stagnant-lid tectonics in early Earth revealed by ^{142}Nd variations in late Archean rocks.
1009 Earth and Planetary Science Letters **373**: 83-92.
1010 Delano, J.W., 2001. Redox History of the Earth's Interior since ~3900 Ma: Implications for Prebiotic
1011 Molecules. Origins of life and evolution of the biosphere **31**(4-5): 311-341.
1012 Evensen, N.M., Hamilton, P.J., and O'Nions, R.K., 1978. Rare earth abundances in chondritic
1013 meteorites. Geochimica et Cosmochimica Acta **42**(8): 1199-1212.
1014 Farquhar, J., Bao, H., and Thiemens, M., 2000. Atmospheric influence of Earth's earliest sulfur cycle.
1015 Science **289**(5480): 756-758.
1016 Fischer-Gödde, M., Becker, H., and Wombacher, F., 2010. Rhodium, gold and other highly siderophile
1017 element abundances in chondritic meteorites. Geochimica et Cosmochimica Acta **74**(1): 356-
1018 379.
1019 Fonseca, R.O.C., Laurenz, V., Mallmann, G., Luguet, A., Hoehne, N., and Jochum, K.P., 2012. New
1020 constraints on the genesis and long-term stability of Os-rich alloys in the Earth's mantle.
1021 Geochimica et Cosmochimica Acta **87**: 227-242.
1022 Fonseca, R.O.C., Mallmann, G., O'Neill, H.S.C., Campbell, I.H., and Laurenz, V., 2011. Solubility of
1023 Os and Ir in sulfide melt: Implications for Re/Os fractionation during mantle melting. Earth and
1024 Planetary Science Letters **311**(3-4): 339-350.
1025 Foster, J.G., Lambert, D.D., Frick, L.R., and Maas, R., 1996. Re-Os isotopic evidence for genesis of
1026 Archaean nickel ores from uncontaminated komatiites. Nature **382**(6593): 703-706.
1027 Fujimaki, H., Tatsumoto, M., and Aoki, K., 1984. Partition coefficient of Hf, Zr and REE between
1028 phenocrysts and groundmasses. Journal of Geophysical Research **89**: 662-672.
1029 Galer, S.J.G., and Goldstein, S.L., 1991. Early mantle differentiation and its thermal consequences.
1030 Geochimica et Cosmochimica Acta **55**(1-2): 227-239.
1031 Goldstein, S.L., Onions, R.K., and Hamilton, P.J., 1984. A Sm-Nd Isotopic Study of Atmospheric Dusts
1032 and Particulates from Major River Systems. Earth and Planetary Science Letters **70**(2): 221-236.
1033 Green, M.G., Sylvester, P.J., and Buick, R., 2000. Growth and recycling of early Archaean continental
1034 crust: geochemical evidence from the Coonterunah and Warrawoona Groups, Pilbara Craton,
1035 Australia. Tectonophysics **322**(1-2): 69-88.
1036 Guitreau, M., Blichert-Toft, J., Martin, H., Mojzsis, S.J., and Albarède, F., 2012. Hafnium isotope
1037 evidence from Archean granitic rocks for deep-mantle origin of continental crust. Earth and
1038 Planetary Science Letters **337-338**: 211-223.

1039 Hamilton, P.J., O'Nions, R.K., Bridgwater, D., and Nutman, A.P., 1983. Sm-Nd studies of Archaean
1040 metasediments and metavolcanics from West Greenland and their implications for the Earth's
1041 early history. Earth and Planetary Science Letters **62**(2): 263-272.
1042 Heaman, L.M., 1997. Global mafic magmatism at 2.45 Ga: Remnants of an ancient large igneous
1043 province? Geology **25**(4): 299-302.
1044 Herzberg, C., Condie, K., and Korenaga, J., 2010. Thermal history of the Earth and its petrological
1045 expression. Earth and Planetary Science Letters **292**(1-2): 79-88.
1046 Hofmann, A.W., 1988. Chemical differentiation of the Earth: The relationship between mantle,
1047 continental crust and oceanic crust. Earth and Planetary Science Letters **90**(3): 297-314.
1048 Horan, M.F., Walker, R.J., Morgan, J.W., Grossman, J.N., and Rubin, A.E., 2003. Highly siderophile
1049 elements in chondrites. Chemical Geology **196**(1-4): 5-20.
1050 Irving, A.J., and Frey, F.A., 1978. Distribution of trace elements between garnet megacrysts and host
1051 volcanic liquids of kimberlitic to rhyolitic composition. Geochimica et Cosmochimica Acta
1052 **42**(NA6): 771-787.
1053 Jacobsen, S.B., and Wasserburg, G.J., 1980. Sm-Nd isotopic evolution of chondrites. Earth and
1054 Planetary Science Letters **50**(1): 139-155.
1055 Jahn, B.M., Vidal, P., and Kröner, A., 1984. Multi-chronometric ages and origin of Archaean tonalitic
1056 gneisses in Finnish Lapland: a case for long crustal residence time. Contributions to Mineralogy
1057 and Petrology **86**(4): 398-408.
1058 Kato, Y., and Nakamura, K., 2003. Origin and global tectonic significance of Early Archean cherts from
1059 the Marble Bar greenstone belt, Pilbara Craton, Western Australia. Precambrian Research **125**(3-
1060 4): 191-243.
1061 Keays, R.R., 1995. The role of komatiitic and picritic magmatism and S-saturation in the formation of
1062 ore deposits. Lithos **34**(1-3): 1-18.
1063 Kennedy, A.K., Lofgren, G.E., and Wasserburg, G.J., 1993. An experimental study of trace element
1064 partitioning between olivine, orthopyroxene, and melt in chondrules: Equilibrium values and
1065 kinetic effects. Earth and Planetary Science Letters **115**(1-4): 177-195.
1066 Kimura, K., Lewis, R.S., and Anders, S., 1974. Distribution of gold and rhenium between nickel-iron
1067 and silicate melts; implications for abundance of siderophile elements on the earth and moon.
1068 Geochimica et Cosmochimica Acta **38**(5): 683-701.
1069 Kleine, T., Mezger, K., Münker, C., Palme, H., and Bischoff, A., 2004. ^{182}Hf-^{182}W isotope systematics
1070 of chondrites, eucrites, and martian meteorites: Chronology of core formation and early mantle
1071 differentiation in Vesta and Mars. Geochimica et Cosmochimica Acta **68**(13): 2935-2946.
1072 König, S., Münker, C., Hohl, S., Paulick, H., Barth, A.R., Lagos, M., Pfander, J., and Büchl, A., 2011.
1073 The Earth's tungsten budget during mantle melting and crust formation. Geochimica et
1074 Cosmochimica Acta **75**(8): 2119-2136.
1075 Kulikov, V.S., Bychkova, Y.V., Kulikova, V.V., and Ernst, R., 2010. The Vetreny Poyas (Windy Belt)
1076 subprovince of southeastern Fennoscandia: An essential component of the ca. 2.5-2.4 Ga Sumian
1077 large igneous provinces. Precambrian Research **183**(3): 589-601.
1078 Kulikov, V.S., Simon, A.K., Kulikova, V.V., Samsonov, A.V., Kajrjak, A.I., Ganin, V.A., and Sudin,
1079 A.I. (1990). Evolution of Archaean magmatism in the Vodla Block, Karelian granite-greenstone
1080 terrane. Precambrian Geology and Geochronology of the East European Platform. Lobach-
1081 Zhuchenko, S.B. and Bibikova, E.V. Leningrad, Nauka**:** 92-100.
1082 Kulikova, V.V. (1993). The Volotsk suite as a type section of the Lower Archean in the Baltic Shield.
1083 Petrozavodsk, Karelian Center RAS Spec. Publ.

Li, Z.X.A., and Lee, C.T.A., 2004. The constancy of upper mantle fO_2 through time inferred from V/Sc ratios in basalts. Earth and Planetary Science Letters **228**(3-4): 483-493.

Lobach-Zhuchenko, S.B., Chekulaev, V.P., Sergeev, S.A., Levchenkov, O.A., and Krylov, I.N., 1993. Archaean rocks from southeastern Karelia (Karelian granite-greenstone terrain). Precambrian Research **62**(4): 375-397.

Lorand, J.-P., and Alard, O., 2001. Platinum-group element abundances in the upper mantle: new constraints from in situ and whole-rock analyses of Massif Central xenoliths (France). Geochimica et Cosmochimica Acta **65**(16): 2789-2806.

Ludwig, K.R. (2003). ISOPLOT 3.00. A geochronological toolkit for Microsoft Excel. Berkeley Geochronology Center Spec. Publ. **No. 4:** 70 pp.

Luguet, A., Shirey, S.B., Lorand, J.-P., Horan, M.F., and Carlson, R.W., 2007. Residual platinum-group minerals from highly depleted harzburgites of the Lherz massif (France) and their role in HSE fractionation of the mantle. Geochimica et Cosmochimica Acta **71**(12): 3082-3097.

Machado, N., Brooks, C., and Hart, S.R., 1986. Determination of initial $^{87}Sr/^{86}Sr$ and $^{143}Nd/^{144}Nd$ in primary minerals from mafic and ultramafic rocks: experimental procedure and implications for the isotopic characteristics of the Archaean mantle under the Abitibi greenstone belt, Canada. Geochimica et Cosmochimica Acta **50**(10): 2335-2348.

Maier, W.D., Barnes, S.J., Campbell, I.H., Fiorentini, M.L., Peltonen, P., Barnes, S.J., and Smithies, R.H., 2009. Progressive mixing of meteoritic veneer into the early Earth's deep mantle. Nature **460**(7255): 620-623.

Martin, H., Chauvel, C., Jahn, B.-M., and Vidal, P., 1983. Rb-Sr and Sm-Nd ages and isotopic geochemistry of Archean granodioritic gneisses from Eastern Finland. Precambrian Research **20**(1): 79-91.

Mertzman, S.A., 2000. K-Ar results from the southern Oregon - northern California Cascade range. Oregon Geology **62**(4): 99-122.

Morgan, J.W., 1985. Osmium isotope constraints on Earth's late accretionary history. Nature **317**(6039): 703-705.

Moyen, J.-F., and Martin, H., 2012. Forty years of TTG research. Lithos **148**: 312-336.

Nesbitt, R.W., and Sun, S.S., 1976. Geochemistry of Archaean spinifex-textured peridotites and magnesian and low-magnesian tholeiites. Earth and Planetary Science Letters **31**(3): 433-453.

Nisbet, E.G., Cheadle, M.J., Arndt, N.T., and Bickle, M.J., 1993. Constraining the potential temperature of the Archaean mantle: A review of the evidence from komatiites. Lithos **30**(3-4): 291-307.

Peucker-Ehrenbrink, B., and Jahn, B.-M., 2001. Rhenium-osmium isotope systematics and platinum group element concentrations: Loess and the upper continental crust. Geochemistry Geophysics Geosystems **2**: Art. No. 2001GC000172.

Puchtel, I.S., Blichert-Toft, J., Touboul, M., Walker, R.J., Byerly, G., Nisbet, E.G., and Anhaeusser, C.R., 2013. Insights into early Earth from Barberton komatiites: Evidence from lithophile isotope and trace element systematics. Geochimica et Cosmochimica Acta **108**: 63-90.

Puchtel, I.S., Brandon, A.D., and Humayun, M., 2004a. Precise Pt-Re-Os isotope systematics of the mantle from 2.7-Ga komatiites. Earth and Planetary Science Letters **224**(1-2): 157-174.

Puchtel, I.S., Brandon, A.D., Humayun, M., and Walker, R.J., 2005. Evidence for the early differentiation of the core from Pt-Re-Os isotope systematics of 2.8-Ga komatiites. Earth and Planetary Science Letters **237**(1-2): 118-134.

Puchtel, I.S., Brügmann, G.E., Hofmann, A.W., Kulikov, V.S., and Kulikova, V.V., 2001. Os isotope systematics of komatiitic basalts from the Vetreny belt, Baltic Shield: Evidence for a chondritic source of the 2.45 Ga plume. Contributions to Mineralogy and Petrology **140**(5): 588-599.

1130 Puchtel, I.S., Haase, K.M., Hofmann, A.W., Chauvel, C., Kulikov, V.S., Garbe-Schönberg, C.D., and
1131 Nemchin, A.A., 1997. Petrology and geochemistry of crustally contaminated komatiitic basalts
1132 from the Vetreny Belt, southeastern Baltic Shield: Evidence for an early Proterozoic mantle
1133 plume beneath rifted Archean continental lithosphere. Geochimica et Cosmochimica Acta **61**(6):
1134 1205-1222.
1135 Puchtel, I.S., Hofmann, A.W., Mezger, K., Jochum, K.P., Shchipansky, A.A., and Samsonov, A.V.,
1136 1998. Oceanic plateau model for continental crustal growth in the Archaean: A case study from
1137 the Kostomuksha greenstone belt, NW Baltic Shield. Earth and Planetary Science Letters **155**(1-
1138 2): 57-74.
1139 Puchtel, I.S., Hofmann, A.W., Mezger, K., Shchipansky, A.A., Kulikov, V.S., and Kulikova, V.V.,
1140 1996. Petrology of a 2.41 Ga remarkably fresh komatiitic basalt lava lake in Lion Hills, central
1141 Vetreny Belt, Baltic Shield. Contributions to Mineralogy and Petrology **124**: 273-290.
1142 Puchtel, I.S., and Humayun, M., 2001. Platinum group element fractionation in a komatiitic basalt lava
1143 lake. Geochimica et Cosmochimica Acta **17**(65): 2979-2993.
1144 Puchtel, I.S., and Humayun, M., 2005. Highly siderophile element geochemistry of ^{187}Os-enriched 2.8-
1145 Ga Kostomuksha komatiites, Baltic Shield. Geochimica et Cosmochimica Acta **69**(6): 1607-
1146 1618.
1147 Puchtel, I.S., Humayun, M., Campbell, A., Sproule, R., and Lesher, C.M., 2004b. Platinum group
1148 element geochemistry of komatiites from the Alexo and Pyke Hill areas, Ontario, Canada.
1149 Geochimica et Cosmochimica Acta **68**(6): 1361-1383.
1150 Puchtel, I.S., Humayun, M., and Walker, R.J., 2007. Os-Pb-Nd isotope and highly siderophile and
1151 lithophile trace element systematics of komatiitic rocks from the Volotsk suite, SE Baltic Shield.
1152 Precambrian Research **158**(1-2): 119-137.
1153 Puchtel, I.S., Walker, R.J., Anhaeusser, C.R., and Gruau, G., 2009a. Re-Os isotope systematics and HSE
1154 abundances of the 3.5 Ga Schapenburg komatiites, South Africa: Hydrous melting or prolonged
1155 survival of primordial heterogeneities in the mantle? Chemical Geology **262**(3-4): 355-369.
1156 Puchtel, I.S., Walker, R.J., Brandon, A.D., and Nisbet, E.G., 2009b. Pt-Re-Os and Sm-Nd isotope and
1157 HSE and REE systematics of the 2.7 Ga Belingwe and Abitibi komatiites. Geochimica et
1158 Cosmochimica Acta **73**(20): 6367-6389.
1159 Puchtel, I.S., Walker, R.J., Touboul, M., Nisbet, E.G., and Byerly, G.R., 2014. Insights into Early Earth
1160 from the Pt-Re-Os isotope and Highly Siderophile Element abundance systematics of Barberton
1161 komatiites. Geochimica et Cosmochimica Acta **125**: 394-413.
1162 Rapp, R.P., Watson, E.B., and Miller, C.F., 1991. Partial melting of amphibolite/eclogite and the origin
1163 of Archean trondhjemites and tonalites. Precambrian Research **51**(1-4): 1-25.
1164 Rehkämper, M., and Halliday, A.N., 1997. Development and application of new ion-exchange
1165 techniques for the separation of the platinum-group and other siderophile elements from
1166 geological samples. Talanta **44**(4): 663-672.
1167 Révillon, S., Hallot, E., Arndt, N.T., Chauvel, C., and Duncan, R.A., 2000. A complex history for the
1168 Caribbean plateau: Petrology, Geochemistry, and geochronology of the Beata Ridge, South
1169 Hispaniola. Journal of Geology **108**(6): 641-661.
1170 Rizo, H., Boyet, M., Blichert-Toft, J., and Rosing, M., 2011. Combined Nd and Hf isotope evidence for
1171 deep-seated source of Isua lavas. Earth and Planetary Science Letters **312**(3-4): 267-279.
1172 Rizo, H., Boyet, M., Blichert-Toft, J., and Rosing, M.T., 2013. Early mantle dynamics inferred from
1173 ^{142}Nd variations in Archean rocks from southwest Greenland. Earth and Planetary Science
1174 Letters **377-378**: 324-335.

1175 Rizo, H., Walker, R.J., Carlson, R.W., Touboul, M., Horan, M.F., Puchtel, I.S., Boyet, M., and Rosing,
1176 M.T., 2016. Early Earth differentiation investigated through ^{142}Nd, ^{182}W, and highly siderophile
1177 element abundances in samples from Isua, Greenland. Geochimica et Cosmochimica Acta **175**:
1178 319-336.
1179 Rudnick, R.L., 1992. Restites, Eu anomalies, and the lower continental crust. Geochimica et
1180 Cosmochimica Acta **56**(3): 963-970.
1181 Rudnick, R.L., and Fountain, D.M., 1995. Nature and composition of the continental crust: a lower
1182 crustal perspective. Reviews of Geophysics **33**(3): 267-309.
1183 Rudnick, R.L., and Gao, S. (2014). Composition of the Continental Crust. Treatise on Geochemistry,
1184 Macmillan Publishers Limited**:** 1-51.
1185 Saunders, A.D., 2005. Large Igneous Provinces: Origin and Environmental Consequences. Elements
1186 **1**(5): 259-263.
1187 Scherer, E., Münker, C., and Mezger, K., 2001. Calibration of the lutetium-hafnium clock. Science
1188 **293**(5530): 683-687.
1189 Shirey, S.B., and Walker, R.J., 1998. The Re-Os isotope system in cosmochemistry and high-
1190 temperature geochemistry. Annual Reviews of Earth and Planetary Sciences **26**: 423-500.
1191 Sisson, T.W., 1994. Trace-element Partitioning with Application to Magmatic Processes Hornblende-
1192 melt trace-element partitioning measured by ion microprobe. Chemical Geology **117**(1): 331-
1193 344.
1194 Smoliar, M.I., Walker, R.J., and Morgan, J.W., 1996. Re-Os ages of Group IIA, IIIA, IVA, and IVB iron
1195 meteorites. Science **271**(5762): 1099-1102.
1196 Söderlund, U., Patchett, J.P., Vervoort, J.D., and Isachsen, C.E., 2004. The ^{176}Lu decay constant
1197 determined by Lu-Hf and U-Pb isotope systematics of Precambrian mafic intrusions. Earth and
1198 Planetary Science Letters **219**(3-4): 311-324.
1199 Thompson, P.M.E., Kempton, P.D., White, R.V., Kerr, A.C., Tarney, J., Saunders, A.D., Fitton, J.G.,
1200 and McBirney, A., 2003. Hf-Nd isotope constraints on the origin of the Cretaceous Caribbean
1201 plateau and its relationship to the Galapagos plume. Earth and Planetary Science Letters **217**(1-
1202 2): 59-75.
1203 Touboul, M., Liu, J., O'Neil, J., Puchtel, I.S., and Walker, R.J., 2014. New Insights into the Hadean
1204 Mantle Revealed by ^{182}W and Highly Siderophile Element Abundances of Supracrustal Rocks
1205 from the Nuvvuagittuq Greenstone Belt, Quebec, Canada. Chemical Geology(383): 63-75.
1206 Touboul, M., Puchtel, I.S., and Walker, R.J., 2012. ^{182}W Evidence for Long-Term Preservation of Early
1207 Mantle Differentiation Products. Science **335**: 1065-1069.
1208 Touboul, M., Puchtel, I.S., and Walker, R.J., 2015. Tungsten isotopic evidence for disproportional late
1209 accretion to the Earth and Moon. Nature **520**(7548): 530-533.
1210 Touboul, M., and Walker, R.J., 2012. High precision tungsten isotope measurement by thermal
1211 ionization mass spectrometry. INTERNATIONAL JOURNAL OF MASS SPECTROMETRY
1212 **309**: 109-117.
1213 van Acken, D., Brandon, A.D., and Humayun, M., 2011. High-precision osmium isotopes in enstatite
1214 and Rumuruti chondrites. Geochimica et Cosmochimica Acta **75**(14): 4020-4036.
1215 Vervoort, J.D., and Blichert-Toft, J., 1999. Evolution of the depleted mantle: Hf isotope evidence from
1216 juvenile rocks through time. Geochimica et Cosmochimica Acta **63**(3-4): 533-556.
1217 Walker, R.J., Bermingham, K., Liu, J., Puchtel, I.S., Touboul, M., and Worsham, E.A., 2015. In search
1218 of late-stage planetary building blocks. Chemical Geology **411**: 125-142.

Walker, R.J., Horan, M.F., Morgan, J.W., Becker, H., Grossman, J.N., and Rubin, A.E., 2002. Comparative ^{187}Re-^{187}Os systematics of chondrites: Implications regarding early solar system processes. Geochimica et Cosmochimica Acta **66**(23): 4187-4201.

Walker, R.J., Shirey, S.B., and Stecher, O., 1988. Comparative Re-Os, Sm-Nd and Rb-Sr isotope and trace element systematics for Archean komatiite flows from Munro Township, Abitibi belt, Ontario. Earth and Planetary Science Letters **87**(1-2): 1-12.

Willbold, M., Elliott, T., and Moorbath, S., 2011. The tungsten isotopic composition of the Earth's mantle before the terminal bombardment. Nature **477**(7363): 195-198.

Willbold, M., Mojzsis, S.J., Chen, H.W., and Elliott, T., 2015. Tungsten isotope composition of the Acasta Gneiss Complex. Earth and Planetary Science Letters **419**: 168-177.

Zindler, A. (1982). Nd and Sr isotopic studies of komatiites and related rocks. Komatiites. Arndt, N.T. and Nisbet, E.G. London, George Allen and Unwin**:** 399-420.

Figure captions

Fig. 1. Schematic integrated section through Victoria's lava lake showing the textural variations and location of the samples analyzed in this study.

Fig. 2. Variations of abundances of selected minor and lithophile trace elements (in ppm, except for W, which is in ppb) in whole-rock samples and olivine separates from Victoria's lava lake as a function of MgO contents (wt.%).

Fig. 3. Bulk Silicate Earth-normalized abundances of selected lithophile trace elements in komatiitic basalts from Victoria's lava lake (a) and tonalites of the Vodla Block (b). Normalizing values are from Hofmann (1988)

Fig. 4. CI chondrite-normalized HSE abundances in whole-rock samples and olivine and chromite separates from Victoria's lava lake and whole-rock samples of Vodla Block tonalites. Normalizing values are from Horan *et al.* (2003)

Fig. 5. Variations of HSE abundances (ppb) as a function of MgO contents (wt.%) in whole-rock samples and olivine separates from Victoria's lava lake.

Fig. 6a. Re-Os isochron diagram for whole-rock komatiitic basalt samples and olivine and chromite separates from Victoria's lava lake.
b. Close-up of the left lower corner of the Re-Os isochron diagram (**a**) showing only samples with low Re/Os ratios.

Fig. 7. Pt-Os isotopic data for the chromite separates from Victoria's lava lake.

Fig. 8. $\mu^{182}W$ values for the localities studied to date, including Victoria's lava lake komatiitic basalts and Vodla Block tonalites from this study. The lava lake W isotopic data were corrected for crustal contamination, as specified in the text. The uncertainties are 2SD. The band for the modern accessible mantle represents the 2SD uncertainty on the Alfa Aesar W standard measured during the course of the present analytical campaign (±4.5 ppm). The sources of the data are as follows: Acasta gneisses: Willbold *et al.* (2015); Isua GB: Willbold *et al.* (2011), Rizo *et al.* (2016); Nuvvuagittuq GB: Touboul *et al.* (2014); the Komati Formation of the Barberton and Kostomuksha GB: Touboul *et al.* (2012).

Fig. 9. $^{142}Nd/^{144}Nd$ data for the Vetreny komatiitic basalts and Vodla Block tonalites. The ^{142}Nd data for the Nd standard AMES and the USGS SRM BCR-1 analyzed at *IGL* are plotted as points of reference.

Fig. 10. Lu-Hf isochron diagram for Victoria's lava lake whole-rock komatiitic basalt samples and pyroxene separates. The reported initial $\varepsilon^{176}Hf$ value is derived from the isochron.

Fig. 11. Variations of calculated initial $\varepsilon^{143}Nd$ values in komatiitic basalts collected from various stratigraphic levels in the Vetreny Belt vs. Eu/Eu* and $(La/Sm)_N$. Since both the Bulk Continental Crust and Archean Continental Crust estimates are characterized by negative Eu anomalies (Rudnick, 1992; Rudnick and Fountain, 1995; Rudnick and Gao, 2014), these correlations are best explained by variable amounts of crustal material added to the original Vetreny komatiite magma. Because komatiites cannot have primary Eu anomalies, these correlations are used to estimate the initial Nd isotopic composition of the original Vetreny komatiite magma $\varepsilon^{143}Nd(T) = +3.7\pm0.3$, as well as the degree of LREE-depletion $(La/Sm)_N$. = 0.41±0.07. These data are further used to estimate the degree of crustal contamination of Victoria's lava lake. See text for details.

Fig. 12. Diagram illustrating the variations of time-integrated Sm/Nd and Lu/Hf ratios in the mantle sources of komatiitic and basaltic systems of various ages. The Sm/Nd and Lu/Hf ratios were calculated using either a two-stage differentiation model for the Komati and Weltevreden systems (Puchtel et al., 2013), or a single-stage model for the rest of the systems (Blichert-Toft and Puchtel, 2010). The sources of the data are as follows. Gorgona komatiites: Aitken and Echeverria (1984), Révillon *et al.* (2000), Thompson *et al.* (2003); Ottawa Islands: Blichert-Toft and Arndt (1999); Birimian terrane: Abouchami *et al.* (1990), Blichert-Toft *et al.* (1999); Belingwe: Blichert-Toft and Arndt (1999), Puchtel *et al.* (2009b); Abitibi: Zindler (1982), Machado *et al.* (1986), Walker *et al.* (1988), Blichert-Toft and Arndt (1999); Kostomuksha: Puchtel *et al.* (1998), Blichert-Toft and Puchtel (2010); Komati and Weltevreden: Puchtel *et al.* (2013). The Chondritic Uniform Reservoir (CHUR) and Depleted MORB Mantle (DM) parameters are from Jacobsen and Wasserburg (1980), Hamilton *et al.* (1983), Goldstein *et al.* (1984), Vervoort and Blichert-Toft (1999), and Bouvier *et al.* (2008).

Fig. 13. Results of model calculations for the composition of the Vodla Block tonalites *via* melting of a mafic crustal source. Tonalite Melt 1, which is most similar to the composition of tonalite sample K04, is calculated to be derived from 10% partial melting of a basaltic source with a composition of Mafic Crust 1, in equilibrium with a Cpx (70%) + Gar (15%) + Hbl (10%) + Rut (5%) residual mineral assemblage at pressures between 12 and 20 Kb. Tonalite Melt 2, which is most similar to the composition of tonalite sample K14, is calculated to have been derived from 10% partial melting of a basaltic source with the composition of Mafic Crust 2, in equilibrium with a Cpx (50%) + Pl (20%)+ Hbl (20%) + TiMgt (7%) + Gar (3%) mineral assemblage and pressures of ~10 Kb. Partition coefficients are from Irving and Frey (1978), Fujimaki *et al.* (1984), Bacon and Druitt (1988), and Sisson (1994). The CI-chondrite normalizing values are from Evensen *et al.* (1978). The two mafic crust compositions are similar to those of the two 3.5 Ga tholeiite sequences from the Warrawoona Group, East Pilbara Craton, Western Australia (Green *et al.*,

2000; Kato and Nakamura, 2003) and represent our best proxies for the mafic crust the Vodla Block tonalites were derived from.

Fig. 14a. Initial $^{187}Os/^{188}Os$ isotopic compositions, expressed in terms of $\gamma^{187}Os$, of the best studied Archean komatiite systems plotted as a function of age. The data for the komatiite systems are from Foster *et al.* (1996), Puchtel *et al.* (2004a, 2005, 2007, 2009a, 2009b, 2014) and this study. The data for chondritic meteorites are compiled from Walker *et al.* (2002), Brandon *et al.* (2005) and Fischer-Gödde *et al.* (2010).
b. Initial $^{186}Os/^{188}Os$ isotopic compositions, expressed in terms of $\varepsilon^{186}Os$, of Archean komatiite systems studied to date, plotted as a function of age. The data are from Puchtel *et al.* (2004a, 2005, 2009b, 2014) and this study. The data for chondritic meteorites are compiled from Horan *et al.* (2003), Brandon *et al.* (2005, 2006), and Fischer-Gödde *et al.* (2010). Note that, whereas the late Archean systems, except for Kostomuksha, plot well within the range of known chondritic meteorites, the early Archean komatiite systems plot outside this range. The uncertainties on the Os initial isotopic ratios are 2SE.

Fig. 15. Calculated total Pt+Pd abundances in the sources of Archean komatiite systems plotted as *per cent* of the total Pt+Pd abundances in the estimates for the modern BSE of Becker *et al.* (2006). In the calculations of the totals, the relative weight of Pd contribution to the total was normalized to Pt on the basis of its relative abundance in the CI chondrite Orgueil (Horan et al., 2003), as described in text. The total Pt+Pd abundances present in the sources of the best-studied Archean komatiite systems compiled from the data of Puchtel *et al.* (2004a, 2004b, 2005, 2007, 2009a, 2009b, 2014) and Puchtel and Humayun (2005). Uncertainties are 2SE. See text for details.

Fig. 16. $\mu^{182}W$ *vs.* total calculated HSE abundances in the sources of komatiite systems studied to date relative to those in the present-day BSE. This proportion corresponds to the fraction of the total HSE budget of the BSE added during late accretion assuming an HSE-free mantle prior to late accretion. The W isotopic composition of BSE prior to late accretion is constrained by the $^{182}W/^{184}W$ data for the lunar mantle to be +21±5 ppm (Touboul *et al.*, 2015), with the uncertainty on the pre-late accretion BSE W isotopic composition defined by the uncertainty on the W isotopic composition of the lunar mantle. Estimates of the total HSE contents in the sources of the Kostomuksha and Komati komatiites are from Puchtel and Humayun (2005) and Puchtel *et al.* (2014) and for the original Vetreny komatiite – from this study.

Table 1. HSE abundances (ppb) and Re-Os isotopic data for whole-rock samples and olivine and chromite separates from Victoria's lava lake komatiitic basalts and for tonalites of the Vodla Block

Sample	Re	Os	Ir	Ru	Pt	Pd	$^{187}Re/^{188}Os$	$^{187}Os/^{188}Os$	$\gamma^{187}Os(T)$	$(Os/Ir)_N$	$(Ru/Ir)_N$	$(Pd/Ir)_N$
Victoria's lava lake komatiitic basalts												
01110	0.467	0.1985	0.457	2.44	13.0	12.7	12.05±0.06	0.60509±40	+1.4	0.421	3.65	21.7
01110/1	0.450	0.1963	0.514	2.45	12.7	12.0	11.72±0.06	0.59158±24	+1.2	0.370	3.25	18.3
12101	0.526	0.02723	0.0513	0.647	11.9	12.1	180.0±0.9	7.4768±58	+2.6	0.515	8.62	184
12124	0.557	0.02217	0.0234	0.451	12.9	14.3	322.5±1.6	13.325±10	+18	0.920	13.2	478
01001_A	0.287	0.7091	1.24	6.66	8.05	7.42	1.966±10	0.19249±10	+1.3	0.553	3.66	4.66
01001_B	0.276	0.6828	1.34	6.86	8.22	7.53	1.964±10	0.19246±13	+1.4	0.494	3.50	4.40
01103_A	0.358	1.220	2.16	5.64	10.8	9.88	1.420±7	0.16963±9	+0.9	0.548	1.78	3.57
01103_B	0.386	1.024	2.15	5.94	10.7	9.69	1.830±9	0.18662±11	+1.0	0.462	1.89	3.53
01104_A	0.348	0.6357	1.74	5.70	10.3	9.34	2.671±13	0.22209±12	+2.0	0.353	2.23	4.18
01104_B	0.338	0.7665	1.95	5.56	10.7	9.15	2.142±11	0.20060±12	+2.2	0.380	1.95	3.66
01105_A	0.280	0.6157	1.17	6.54	8.19	7.53	2.215±11	0.20322±12	+1.8	0.512	3.83	5.04
01105_B	0.271	1.036	1.71	7.19	8.68	7.51	1.266±6	0.16558±10	+2.9	0.588	2.88	3.44
01106_A	0.338	0.8405	1.90	5.73	10.2	9.54	1.955±10	0.19298±12	+2.2	0.429	2.07	3.93
01106_B	0.380	0.9683	2.06	6.56	10.1	10.0	1.907±10	0.18991±13	+1.2	0.455	2.18	3.80
01001 Ol	0.00224	0.1177	0.159	5.10	0.297	0.112	0.0916±78	0.11657±9	+2.0	0.716	21.9	0.549
01103 Ol	0.0206	0.5914	0.663	4.78	0.911	0.527	0.1672±22	0.11888±6	+1.3	0.864	4.92	0.621
01104 Ol	0.0276	0.4639	0.748	4.47	1.93	1.28	0.2866±23	0.12519±6	+2.6	0.601	4.08	1.33
01105 Ol_B	0.00952	0.2197	0.319	5.13	0.550	0.313	0.2086±45	0.12075±9	+1.5	0.667	11.0	0.767
01106 Ol	0.0147	0.7155	1.03	5.20	1.44	0.559	0.0989±15	0.11626±7	+1.5	0.674	3.46	0.424
01001 Chr	0.412	29.68	49.9	349	61.4	1.46	0.0668±9	0.11495±7	+1.5	0.576	4.77	0.0229
01105 Chr	0.383	25.51	44.1	344	43.1	1.01	0.0722±8	0.11523±6	+1.5	0.560	5.33	0.0180
12001 Chr1.1	0.268	14.58	24.2	339	29.2	2.90	0.0883±5	0.11614±9	+1.8	0.584	9.57	0.0936
12001 Chr2.1	0.271	13.80	23.0	337	24.4	3.32	0.0946±5	0.11615±10	+1.5	0.581	10.0	0.113
12001 Chr blk	0.285	15.63	25.2	343	21.2	1.97	0.0885±5	0.11588±7	+1.5	0.601	9.3	0.0610
12105 Chr1.1	0.260	12.31	20.2	333	15.0	1.95	0.1015±6	0.11658±8	+1.7	0.592	11.3	0.0756
12105 Chr2.1	0.259	11.67	19.6	340	22.7	2.25	0.1068±6	0.11672±8	+1.6	0.577	11.9	0.090
12105 Chr1.2	0.266	10.46	16.9	331	21.2	2.53	0.1224±7	0.11740±5	+1.7	0.599	13.4	0.1168
12105 Chr blk	0.265	14.94	24.3	355	33.2	3.95	0.0854±5	0.11598±6	+1.7	0.597	9.98	0.1271
Vodla Block tonalites												
K04	0.0219	0.002976	0.00298	0.00420	0.0683	0.0236	47.42±0.29	3.0763±31	+347	0.966	0.961	6.17
K10	0.0118	0.005647	0.00298	0.00924	0.208	0.0149	11.11±0.13	0.9694±10	+242	1.84	2.12	3.90
K13	0.0476	0.005650	0.00381	0.0107	0.125	0.0959	57.76±0.17	3.6195±36	+323	1.44	1.92	19.7

Note. The HSE abundances are re-calculated on an anhydrous basis. The initial $\gamma^{187}Os$ values were calculated at T = 2407 Ma (lava lake) or 3213 Ma (tonalites) using the parameters specified in the text. Normalizing values are from Horan *et al.* (2003).

Table 2. High-precision Os isotopic data and Pt/Os ratios for chromite separates from Victoria's lava lake komatiitic basalts.

Sample	^{190}**Pt/**^{188}**Os**	^{184}**Os/**^{188}**Os**	^{186}**Os/**^{188}**Os**	ε^{186}**Os(*T*)**
01001 Chr	0.001977±10	0.001317±2	0.1198405±21	+0.09±0.18
01105 Chr	0.001614±08	0.001310±5	0.1198383±03	+0.01±0.03
12001 Chr 1.1	0.001912±10	0.001330±5	0.1198395±21	+0.02±0.17
12001 Chr 2.1	0.001687±08	0.001306±1	0.1198390±21	+0.04±0.17
12001 Chr bulk	0.001297±06	0.001302±1	0.1198376±11	+0.05±0.09
12105 Chr 1.1	0.001162±06	0.001306±5	0.1198371±06	+0.04±0.05
12105 Chr 2.1	0.001858±09	0.001301±1	0.1198390±17	-0.01±0.14
12105 Chr 1.2	0.001936±10	0.001303±1	0.1198402±15	+0.07±0.12
12105 Chr bulk	0.002121±11	0.001302±1	0.1198400±17	0.00±0.15

Note. The initial ε^{186}Os values were calculated at the emplacement age T = 2407 Ma. The uncertainties are 2SE.

Table 3. W isotopic compositions and W abundance data for Victoria's lava lake komatiitic basalts and Vodla Block tonalites.

Sample	$\mu^{182}W$	W (ppb)
Victoria's lava lake komatiitic basalts		
01110		66.7±2.0
01110/1	+2.4±3.2	59.3±2.0
01111		48.2±1.8
12116	+6.9±2.2	48.2±1.0
12117	+8.2±1.8	41.6±0.9
12107	+11.1±2.9	64.8±1.0
12108	+5.7±3.1	61.8±1.0
12108*	+3.8±3.6	
12109	+7.2±3.4	68.9±1.0
12109*	+12.9±3.1	
01001_B	+6.8±4.8	36.2±1.6
12001		35.3±0.4
12105		34.6±0.9
01105_B	+5.1±4.3	36.7±1.6
01103_B		35.1±2.1
01104_B	+8.9±4.6	38.6±2.1
12106		37.5±0.8
01106_B	+6.6±4.0	32.7±1.9
Vodla Block tonalites		
K04	+13.1±1.9	78.6±0.8
K10	+15.5±3.1	78.8±1.1
K13	+10.7±2.4	169±2.2
K14	+11.2±2.5	53.6±0.6

Note. *Separate digestions of the same samples. The W abundance data were obtained using isotope dilution ICP-MS on 100 mg aliquots of the same sample powders as used for the isotopic composition measurements. $\mu^{182}W$ denotes ppm deviation of $^{182}W/^{184}W$ measured in the samples from the average value for the terrestrial standard.

Table 4. Sm and Nd concentrations and Sm-Nd isotopic compositions of Victoria's lava lake komatiitic basalts and Vodla Block tonalites

Sample	Sm, ppm	Nd, ppm	$^{147}Sm/^{144}Nd$	$\mu^{142}Nd$	$^{143}Nd/^{144}Nd$	$\varepsilon^{143}Nd(T)$
Victoria's lava lake komatiitic basalts						
01105_A	1.241	5.270	0.1424	+0.4±2.9	0.511734±2	-0.82
12101	2.248	9.617	0.1413	-0.9±2.4	0.511733±2	-0.52
12124	2.505	10.59	0.1430	+0.7±1.7	0.511733±1	-1.0
12107	1.940	8.240	0.1423		0.511733±4	-0.83
12116	2.158	9.177	0.1422	+0.4±1.4	0.511736±1	-0.73
12117	2.123	8.965	0.1432	+2.0±1.9	0.511737±1	-1.0
Vodla Block tonalites						
K04	1.605	11.37	0.08538	+4.1±1.7	0.510387±1	+2.2
K04 replicate				+0.7±2.5	0.510391±2	
K10	2.402	18.68	0.07774	+0.3±2.1	0.510226±1	+2.2
K10 replicate				-4.7±2.0	0.510232±1	
K13	2.409	16.23	0.08975	-1.2±5.1	0.510464±4	+1.9
K13 replicate				+0.6±4.7	0.510465±3	
K14	3.860	22.66	0.10300	-2.9±1.8	0.510696±1	+0.93
K14 replicate				0.0±2.3	0.510699±1	

Note. Initial $\varepsilon^{143}Nd$ values calculated at the time of emplacement of the komatiitic basalts (T = 2407 Ma) and the tonalites (T = 3213 Ma).

1372 **Table 5.** Lu and Hf concentrations and Lu-Hf isotopic compositions of Victoria's lava lake
1373 komatiitic basalts and Vodla Block tonalites.
1374

Sample	Lu (ppm)	Hf (ppm)	$^{176}Lu/^{177}Hf$	$^{176}Hf/^{177}Hf$	$\varepsilon^{176}Hf(T)$
Victoria's lava lake komatiitic basalts					
01001 WR	0.1296	0.8495	0.02166±4	0.282230±10	-0.2
01103 WR	0.1663	1.092	0.02162±4	0.282244±5	+0.3
01104 WR	0.1601	1.086	0.02093±4	0.282211±7	+0.3
01105 WR	0.1285	0.8440	0.02162±4	0.282232±5	-0.1
01106 WR	0.1562	1.017	0.02178±4	0.282270±8	+1.0
01001 Cpx	0.1889	1.082	0.02479±5	0.282385±7	+0.2
01103 Cpx	0.1794	0.7582	0.03358±7	0.282809±10	+0.9
01104 Cpx	0.2072	0.9908	0.02968±6	0.282614±6	+0.3
01105 Cpx	0.1719	0.9899	0.02465±5	0.282390±3	+0.6
12105 Cpx	0.1811	0.9965	0.02580±5	0.282446±5	+0.7
01106 Cpx	0.1778	0.7523	0.03355±7	0.282796±9	+0.5
Vodla Block tonalites					
K04	0.04255	3.082	0.001960±4	0.280890±3	+2.2
K10	0.05996	4.723	0.001802±4	0.280953±3	+4.8
K13	0.1050	4.234	0.003521±7	0.280957±3	+1.1
K14	0.1873	3.843	0.006917±14	0.281194±4	+2.1

1375
1376 **Note.** Initial $\varepsilon^{176}Hf$ values calculated at the emplacement ages T = 2407 Ma (komatiitic basalts)
1377 and 3213 Ma (tonalites).
1378
1379

1380 **Table 6.** Parameters used in modeling crustal contamination of the original Vetreny komatiite
1381 magma with tonalites of the Vodla Block and modeling results
1382

	Nd, ppm	**Hf, ppm**	**^{143}Nd/^{144}Nd @2407 Ma**	**^{176}Hf/^{177}Hf @2407 Ma**
Original Vetreny komatiite magma @27 wt.% MgO	1.44	0.420	0.509705±15 ε^{143}Nd = +3.7±0.3	0.281418±13 ε^{176}Hf = +6.3±0.5
Crustal contaminant at 2.407 Ga (Vodla Block tonalites)	18.4	4.0	0.509032±29 ε^{143}Nd = -9.5±0.6	0.280835±44 ε^{176}Hf = -14.4±1.6
Contaminated Vetreny komatiite @27 wt.% MgO	5.5±0.2	0.97±0.05	0.509471±5 ε^{143}Nd = -0.90±0.09	0.281252±6 ε^{176}Hf = +0.41±0.23

1383

1384

Table 7. Calculated Os isotope compositions, siderophile element abundances (ppb), and MgO (wt.%) contents in the original Vetreny komatiitic magma and its mantle source, and parameters used to model the effect of crustal contamination on the Os and W isotopic composition of the original Vetreny komatiite magma.

	W, ppb	Re, ppb	Os, ppb	Pt, ppb	Pd, ppb	MgO, wt.%	$^{186}Os/^{188}Os_i$	$^{187}Os/^{188}Os_i$
Original Vetreny komatiite magma	14.5±1.8		1.9±0.3	8.6±0.9	8.4±0.9	27	0.1198329±3	0.11199±21
Vetreny komatiite source	8.1±0.9			4.9±0.5	4.8±0.5	38	0.1198329±3	0.11199±21
Bulk Silicate Earth	8.3±7.1	0.35±0.12	3.9±1.0	7.6±2.6	7.1±2.6	38	0.1198325	0.11057
Average VB tonalite	635*	0.0271	0.0048	0.134	0.045	1.4	0.1198625	0.48417
Upper Continental Crust	1900	0.198	0.031	0.510	0.520	2.4	0.1198491	0.52986

Note. *Calculated using the average Th concentration in the VBT of 3.51 ppm and the BCC W/Th = 0.18 from Rudnick and Gao (2014). The estimate of W content in BSE is from Arevalo and McDonough (2008), and the estimates of HSE contents from Becker *et al.* (2006). Uncertainties are 2SE. The initial Os isotopic compositions were calculated at T = 2407 Ma.

1396 **Table 1A**. Selected major- (wt. %), minor, and trace (ppm) element data for whole-rock komatiitic basalt samples
1397 and olivine separates from Victoria's lava lake, for tonalites of the Vodla Block and USGS SRM BIR-1 and BCR-1.

Sample	SiO_2	TiO_2	Al_2O_3	Fe_2O_3	MnO	MgO	CaO	Na_2O	K_2O	P_2O_5	LOI	Cr	V	Co	Ni	Total
01110/1	50.4	0.585	11.4	11.4	0.175	14.7	8.80	1.63	0.75	0.07	2.63	1475	193	67	415	100.26
12110/1	49.8	0.580	11.5	11.7	0.190	14.6	8.87	1.65	0.72	0.07	2.23	1349	194	51	366	99.92
01110	50.7	0.595	11.6	11.4	0.175	13.9	9.11	1.83	0.34	0.07	2.58	1380	194	63	374	99.95
12110	50.6	0.590	11.7	11.7	0.190	13.7	9.04	1.84	0.33	0.09	2.25	1277	200	27	332	99.96
01111	51.1	0.602	11.8	11.6	0.184	13.5	9.16	1.43	0.14	0.07	2.06	1478	205	62	340	100.01
12111	50.3	0.600	11.9	11.9	0.200	13.6	9.18	1.42	0.12	0.07	1.54	1374	199	46	351	99.56
12116	50.9	0.650	13.0	11.7	0.200	11.1	10.3	1.75	0.11	0.09	0.75	845	211	66	341	100.07
01117	50.8	0.664	12.9	11.8	0.211	10.0	10.4	2.02	0.11	0.08	0.54	788	215	71	210	99.17
12117	50.9	0.650	13.1	11.5	0.190	11.2	10.3	1.98	0.10	0.09	0.58	818	206	44	306	100.15
01101	52.0	0.687	13.3	11.3	0.212	8.79	10.8	1.71	0.46	0.10	1.03	536	225	63	131	99.48
12101	51.0	0.670	13.3	11.7	0.200	10.1	10.4	1.92	0.36	0.09	0.74	607	216	54	241	99.90
12124	52.5	0.700	14.3	11.1	0.190	7.42	11.0	2.19	0.53	0.09	0.25	372	249	21	86	100.02
12107	52.7	0.670	14.1	10.9	0.190	7.77	11.6	1.84	0.25	0.09	0.35	479	232	40	186	100.18
12108	52.8	0.700	14.1	10.9	0.180	7.47	11.3	1.84	0.33	0.09	0.46	438	240	29	95	99.79
12109	52.7	0.690	14.2	10.9	0.190	7.46	11.4	1.92	0.26	0.09	0.45	437	243	40	90	99.96
01001_A	46.0	0.369	7.22	12.4	0.184	26.5	5.69	0.89	0.22	0.04	2.44	3258	133	106	1119	100.07
01001_B	46.0	0.401	7.40	12.4	0.195	25.4	5.71	0.93	0.21	0.07	2.78	3148	131	124	1157	99.43
12001	45.8	0.380	7.44	12.4	0.200	26.4	5.85	0.94	0.22	0.06	2.99	3146	134	105	1172	100.32
01103_A	48.7	0.498	9.26	11.8	0.193	20.2	7.48	1.05	0.23	0.08	1.69	2073	151	100	802	99.98
01103_B	48.5	0.497	9.32	11.7	0.193	20.2	7.54	1.02	0.22	0.08	1.49	2090	155	101	721	99.70
01104_A	47.6	0.445	8.62	12.0	0.182	22.4	7.01	1.00	0.28	0.05	1.08	1990	145	85	888	100.04
01104_B	47.9	0.476	8.76	11.8	0.192	21.6	6.96	1.02	0.26	0.08	1.27	1903	146	101	940	99.55
01105_A	46.2	0.379	7.34	12.4	0.184	26.5	5.84	0.92	0.23	0.05	2.32	3295	128	106	1103	100.71
01105_B	46.2	0.401	7.29	12.5	0.195	25.6	5.65	0.95	0.20	0.07	2.80	3099	134	115	1117	99.68
12105	45.8	0.380	7.37	12.3	0.200	26.6	5.88	0.92	0.18	0.06	3.21	3170	138	90	1185	100.41
01106_A	47.8	0.455	8.71	11.8	0.182	22.3	7.17	1.03	0.22	0.05	1.05	1938	142	82	874	100.18
01106_B	47.9	0.467	8.74	12.0	0.183	21.4	7.02	1.03	0.29	0.08	1.42	1918	151	98	875	99.52
12106	47.7	0.480	9.17	11.8	0.190	21.5	7.43	1.07	0.22	0.07	1.06	1933	153	72	1005	100.07
01001 Ol	38.0	0.030	0.97	14.3	0.220	45.4	0.96	0.00	0.00	0.01	n.d.	715	16	192	2175	100.26
01103 Ol	39.5	0.020	0.57	14.0	0.193	44.8	0.53	0.00	0.00	0.01	n.d.	588	20	200	2229	100.06
01104 Ol	37.4	0.100	2.06	16.7	0.239	42.0	1.73	0.00	0.00	0.01	n.d.	712	40	215	2027	100.56
01105 Ol_A	38.7	0.060	1.22	14.9	0.220	43.4	1.33	0.00	0.00	0.01	n.d.	806	20	202	2117	100.22
01105 Ol_B	38.7	0.030	0.80	14.6	0.200	45.1	0.49	0.00	0.00	0.00	n.d.	782	18	200	1973	100.25
01106 Ol	38.0	0.110	0.95	15.4	0.225	43.9	1.41	0.00	0.00	0.01	n.d.	892	32	230	2012	100.43
12001 Ol	39.3	0.014	0.04	13.9	0.188	45.2	0.24	0.00	0.00	0.01	n.d.	591	18	200	2140	99.21
12105 Ol	39.3	0.007	0.04	15.3	0.205	44.1	0.24	0.00	0.00	0.01	n.d.	565	18	200	1953	99.54
K04	67.4	0.270	17.9	2.75	0.040	1.50	4.06	5.34	0.72	0.08	0.63	37	48	<1	12	100.07
K10	70.7	0.350	16.1	2.90	0.040	1.04	3.32	4.48	1.00	0.10	0.51	17	62	<1	7	99.99
K13	68.5	0.370	16.6	3.62	0.050	1.32	3.94	4.74	1.01	0.12	0.49	15	58	<1	5	100.31
K14	66.1	0.350	17.8	3.86	0.060	1.54	4.73	4.87	0.90	0.14	0.60	10	68	<1	2	100.31
BIR-1	47.1	0.946	15.5	11.2	0.18	9.70	13.3	1.78	0.010	0.025	n.d.	417	325	50	140	99.80
BIR-1	47.2	0.939	15.5	11.5	0.17	9.57	13.1	1.79	0.012	0.028	n.d.	417	334	52	134	99.82
BCR-1	53.9	2.28	13.8	13.6	0.20	3.69	7.17	3.22	1.80	0.362	n.d.	16	395	44	15	99.91

1398

Table 1A. *(Continued 1)*

Sample	Th	U	Nb	La	Ce	Pr	Nd	Sm	Eu	Gd	Tb	Dy	Ho
12110/1	1.03	0.222	2.10	6.73	14.5	1.93	8.22	1.96	0.663	2.20	0.353	2.28	0.478
12110	1.07	0.235	2.11	7.09	15.0	1.99	8.52	2.03	0.682	2.27	0.361	2.39	0.502
12116	1.15	0.243	2.30	7.53	16.1	2.14	9.18	2.16	0.705	2.47	0.391	2.54	0.535
12117	1.16	0.253	2.31	7.21	15.7	2.07	8.97	2.12	0.691	2.41	0.383	2.46	0.518
12101	1.17	0.253	2.38	7.73	16.7	2.24	9.69	2.26	0.743	2.60	0.411	2.62	0.546
12124	1.30	0.278	2.60	8.38	18.0	2.38	10.4	2.40	0.817	2.74	0.434	2.80	0.589
01001_B	0.662	0.141	1.34	4.39	9.37	1.25	5.38	1.26	0.414	1.42	0.229	1.46	0.308
12001	0.614	0.145	1.24	4.49	9.36	1.23	5.30	1.24	0.405	1.41	0.224	1.44	0.305
01103_B	0.887	0.196	1.73	5.62	11.4	1.60	6.95	1.65	0.543	1.89	0.302	1.95	0.411
01104_B	0.809	0.171	1.74	5.43	11.1	1.54	6.60	1.55	0.507	1.73	0.274	1.78	0.376
01105_B	0.657	0.138	1.40	4.34	9.13	1.23	5.27	1.24	0.408	1.41	0.225	1.46	0.306
12105	0.593	0.139	1.24	4.33	9.12	1.20	5.13	1.21	0.398	1.38	0.221	1.42	0.298
01106_B	0.762	0.167	1.79	5.17	10.9	1.47	6.35	1.51	0.495	1.71	0.270	1.77	0.376
12106	0.776	0.164	1.66	5.10	10.9	1.47	6.37	1.50	0.500	1.72	0.271	1.77	0.368
12001 Ol	0.00379	0.00294	0.0755	0.0337	0.0952	0.0157	0.0836	0.0260	0.00792	0.0333	0.00575	0.0409	0.00950
12105 Ol	0.00493	0.00335	0.0800	0.0471	0.107	0.0181	0.0932	0.0296	0.0162	0.0401	0.00710	0.0506	0.0113
K04	2.65	0.164	1.92	18.0	31.3	3.38	11.4	1.61	0.741	1.20	0.130	0.639	0.114
K10	4.10	0.260	3.25	32.2	55.4	5.72	18.7	2.40	0.812	1.72	0.181	0.894	0.161
K13	2.80	0.256	4.10	23.7	39.4	4.65	16.2	2.41	0.811	1.97	0.242	1.34	0.260
K14	4.48	0.393	2.97	26.2	58.6	6.19	22.7	3.86	0.889	3.17	0.420	2.43	0.474
BIR-1	0.031	0.011	0.554	0.602	1.88	0.367	2.35	1.08	0.515	1.80	0.355	2.56	0.570
±2SD	0.007	0.003	0.049	0.037	0.12	0.020	0.12	0.05	0.027	0.12	0.020	0.13	0.027
BCR-1	5.99	1.73	13.0	25.6	53.7	6.68	28.9	6.69	2.00	6.84	1.07	6.40	1.29
±2SD	0.16	0.05	0.41	0.6	0.9	0.29	1.0	0.23	0.05	0.11	0.07	0.15	0.04

1401 **Table 1A**. *(Continued 2)*

Sample	Er	Tm	Yb	Lu	Hf	Y	Zr	Sc	Cu	Ga	$(La/Sm)_N$	$(Gd/Yb)_N$	Nb/Nb*
12110/1	1.40	0.203	1.35	0.200	1.45	12.5	49.7	32.1	87.3	12.2	2.16	1.32	0.288
12110	1.46	0.213	1.41	0.208	1.48	12.6	50.7	32.6	90.3	12.5	2.20	1.30	0.278
12116	1.57	0.226	1.51	0.225	1.57	13.6	54.9	35.9	97.3	13.6	2.20	1.33	0.283
12117	1.51	0.220	1.45	0.217	1.60	13.7	55.0	35.5	98.3	13.4	2.14	1.34	0.289
12101	1.60	0.232	1.58	0.229	1.59	14.2	56.9	37.1	99.7	13.8	2.15	1.33	0.287
12124	1.72	0.249	1.65	0.248	1.74	15.2	61.7	39.3	107	15.1	2.19	1.35	0.286
01001_B	0.893	0.129	0.873	0.132	0.861	7.98	31.2	22.6	59.6	8.10	2.20	1.32	0.284
12001	0.893	0.130	0.863	0.129	0.875	7.80	31.7	22.4	60.0	8.15	2.27	1.32	0.271
01103_B	1.20	0.174	1.17	0.172	1.18	10.4	41.2	28.2	71.4	10.0	2.14	1.31	0.281
01104_B	1.10	0.158	1.06	0.159	1.06	10.0	38.5	26.7	73.4	9.86	2.21	1.32	0.300
01105_B	0.886	0.131	0.875	0.131	0.899	8.33	32.0	23.2	58.9	8.40	2.20	1.30	0.301
12105	0.868	0.128	0.848	0.127	0.881	7.70	30.6	22.6	57.8	7.92	2.26	1.32	0.281
01106_B	1.09	0.156	1.05	0.159	1.05	9.77	40.0	27.7	68.2	9.40	2.16	1.32	0.326
12106	1.08	0.158	1.05	0.158	1.04	9.32	40.0	27.3	68.7	9.71	2.14	1.32	0.303
12001 Ol	0.0312	0.00543	0.0428	0.00813	0.0170	0.283	1.12	0.283	6.49	0.242	0.817	0.627	2.42
12105 Ol	0.0373	0.00625	0.0483	0.00862	0.0261	0.326	1.23	0.326	4.04	0.289	1.002	0.671	1.90
K04	0.296	0.0391	0.270	0.0405	2.73	2.82	100	2.82	24.9	21.0	7.07	3.58	0.100
K10	0.423	0.0557	0.364	0.0588	4.47	4.09	186	4.09	10.0	18.6	8.45	3.81	0.102
K13	0.739	0.106	0.695	0.105	4.11	6.92	151	6.92	20.1	20.2	6.19	2.29	0.182
K14	1.36	0.195	1.28	0.183	3.93	12.4	163	12.4	45.6	21.3	4.27	2.01	0.099
BIR-1	1.70	0.250	1.66	0.248	0.594	14.8	14.9	43.6	124	15.7	0.557	1.09	1.48
±2SD	0.09	0.013	0.09	0.013	0.041	0.6	2.3	2.0	6	0.6	0.018	0.04	0.13
BCR-1	3.63	0.538	3.42	0.507	5.04	35.9	189	32.0	20.8	23.2	2.41	1.62	0.380
±2SD	0.06	0.016	0.09	0.019	0.08	1.9	13	1.4	3.2	0.6	0.03	0.02	0.014

1402 **Note.** *Average of two replicate analyses. A and B are splits of the same crush for each of the whole-rock
1403 cumulate samples. The whole-rock analyses are re-calculated on an anhydrous basis. n.d. – not determined. Major
1404 and minor element data obtained *via* XRF mass-spectrometry.
1405

1406

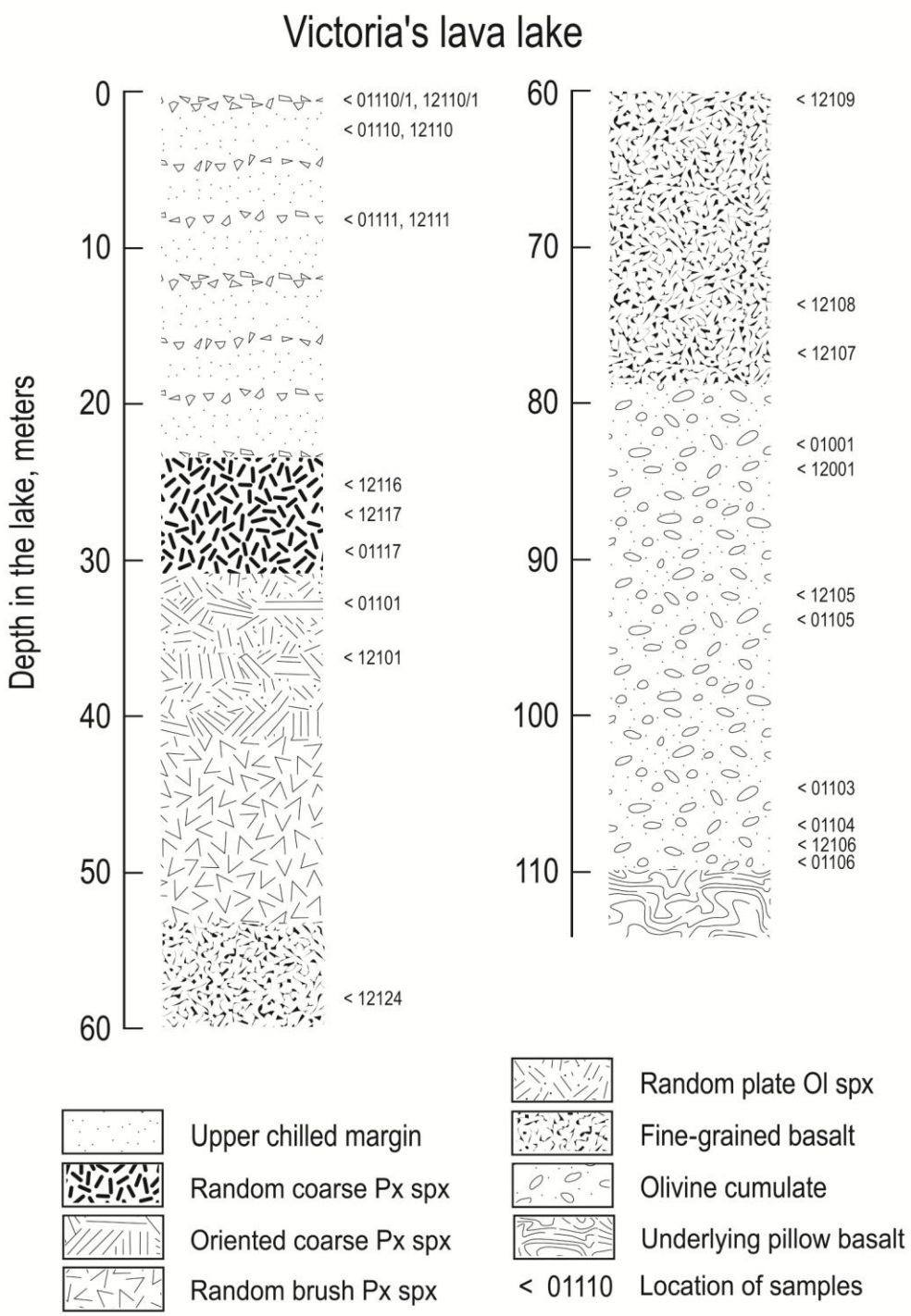

1407

1408 **Fig. 1.**

1409

1410

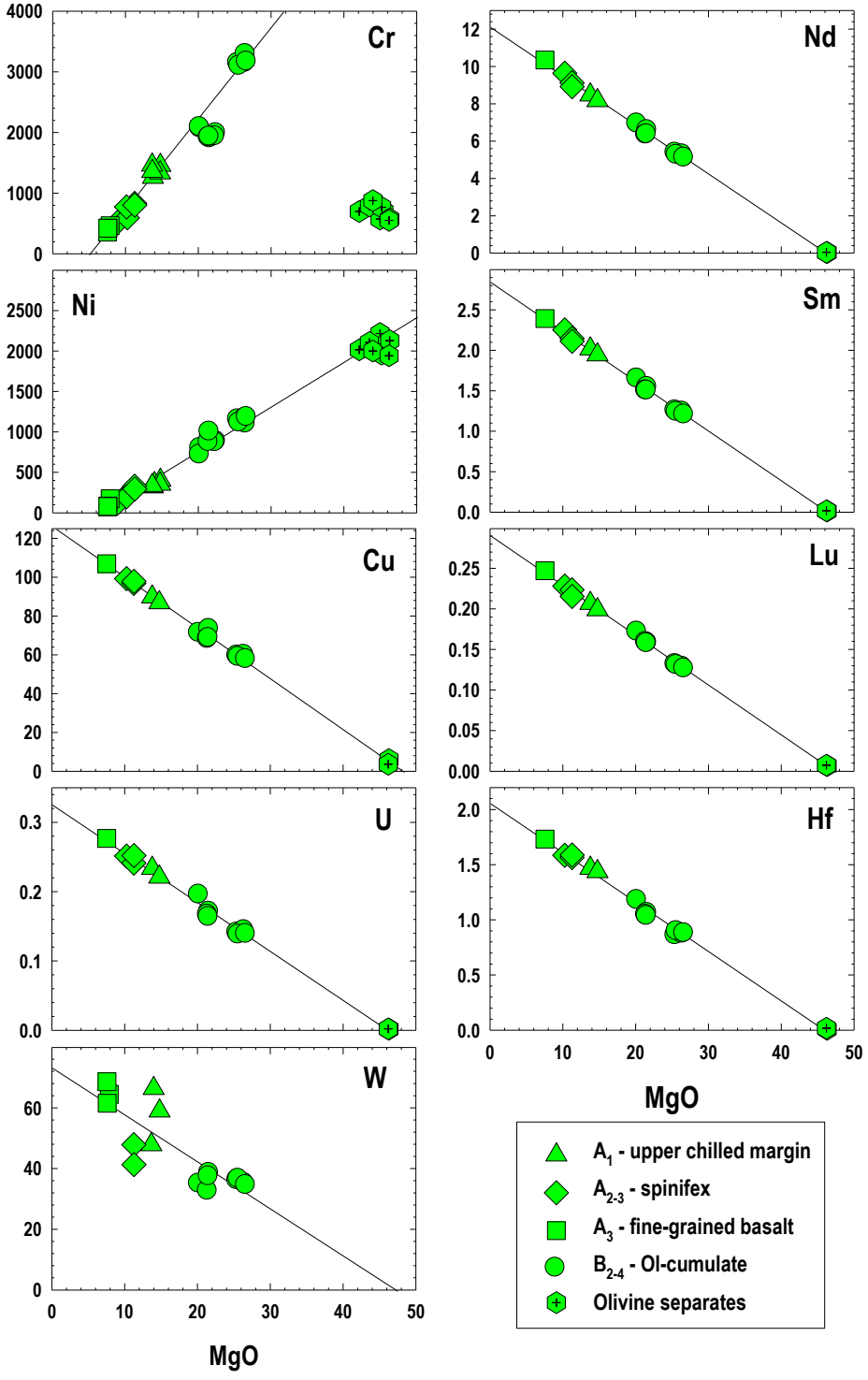

1411

1412 **Fig. 2.**

1413

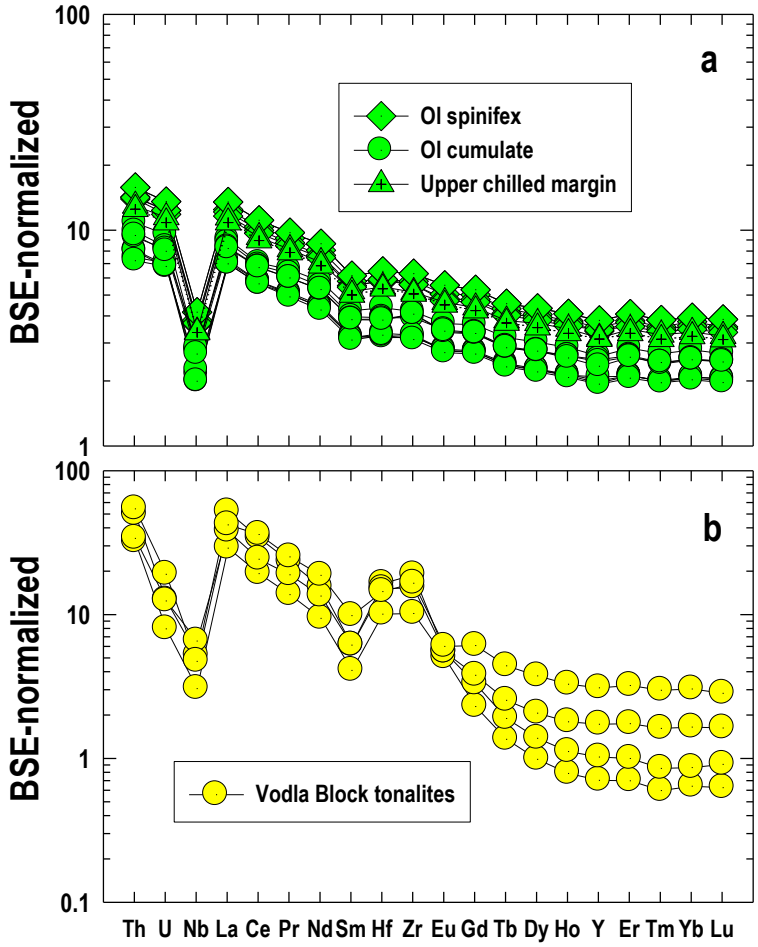

1414

1415 **Fig. 3.**

1416

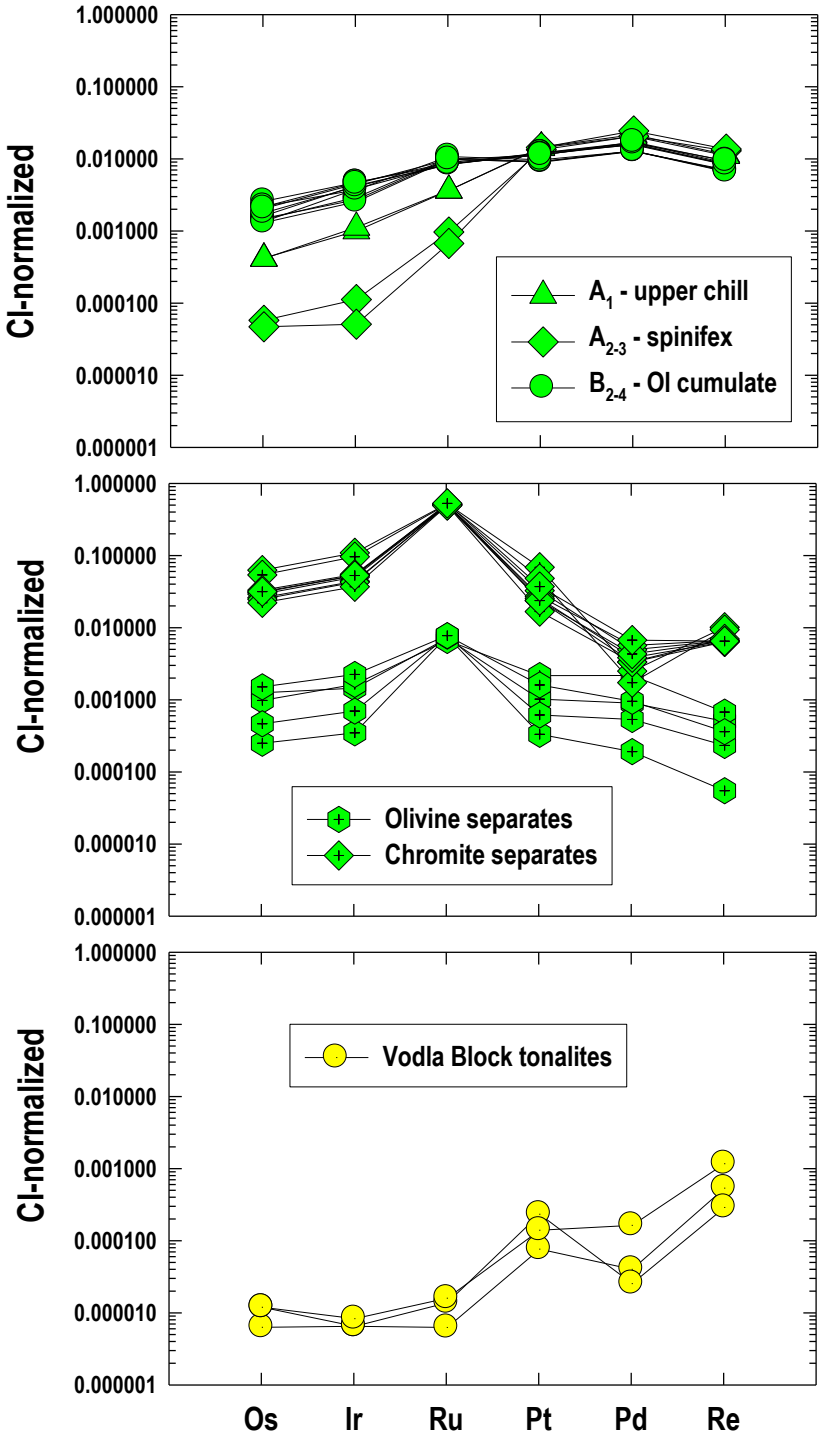

1417

1418 **Fig. 4.**

1419

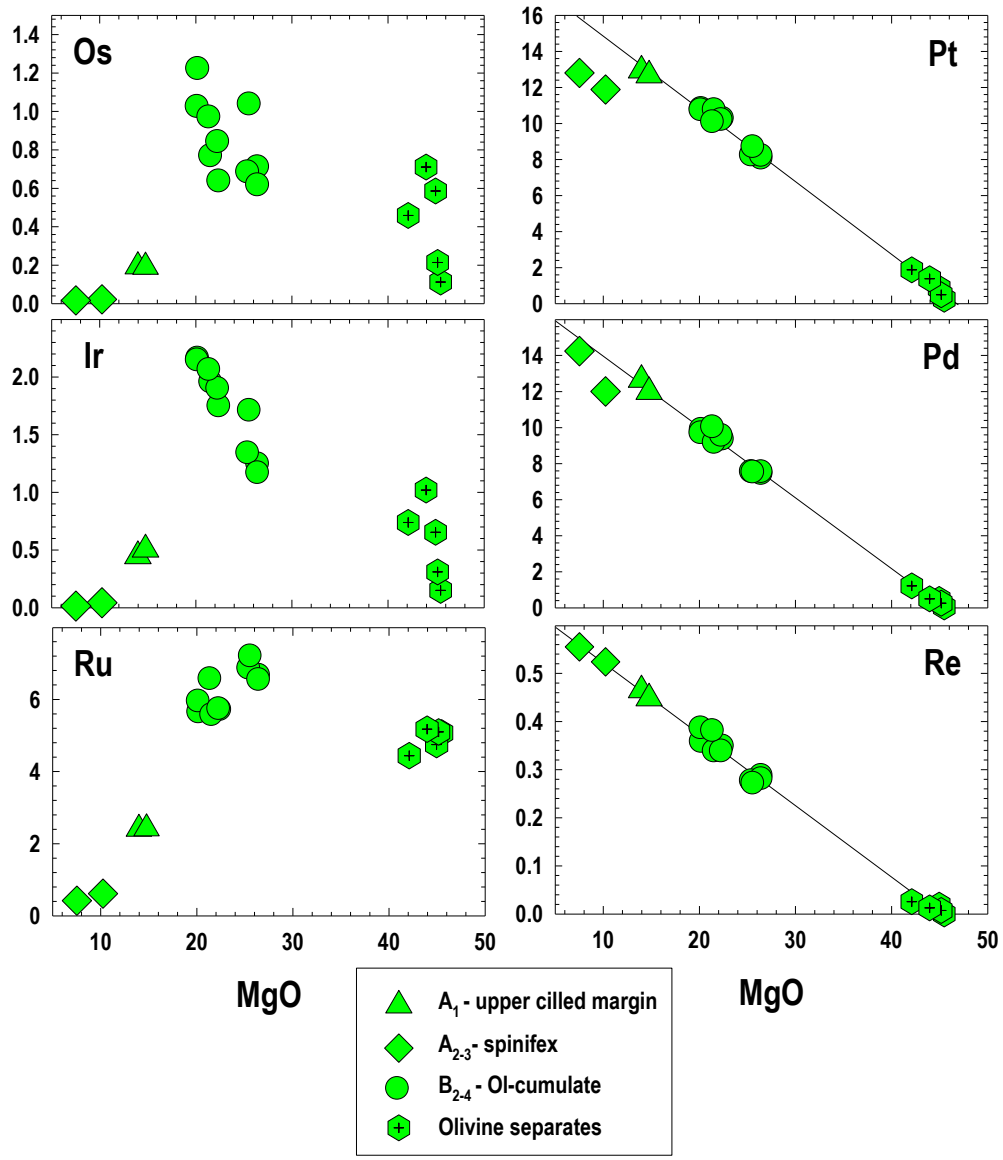
Os
Pt
Ir
Pd
Ru
Re
MgO
MgO
A1 - upper cilled margin
A2-3 - spinifex
B2-4 - Ol-cumulate
Olivine separates

Fig. 5.

1424

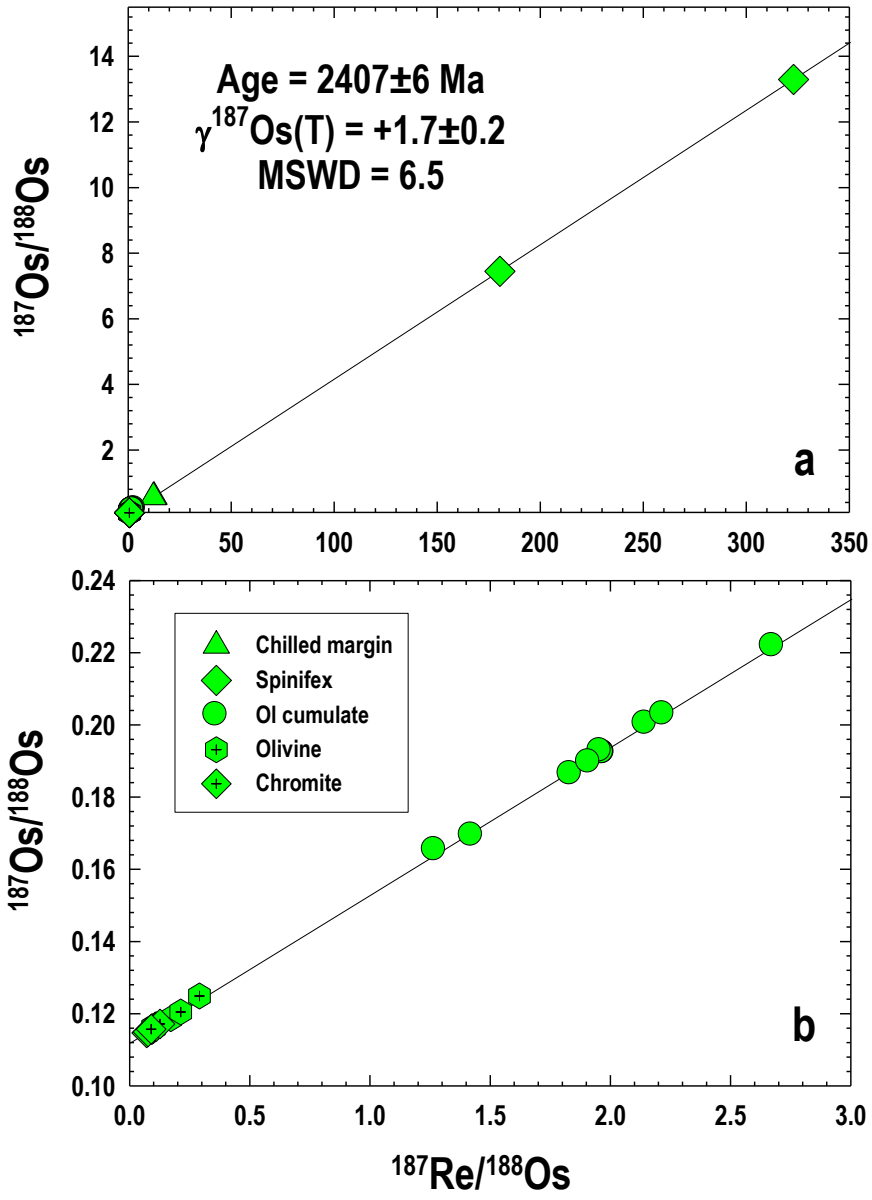

1425

1426 **Fig. 6.**

1427

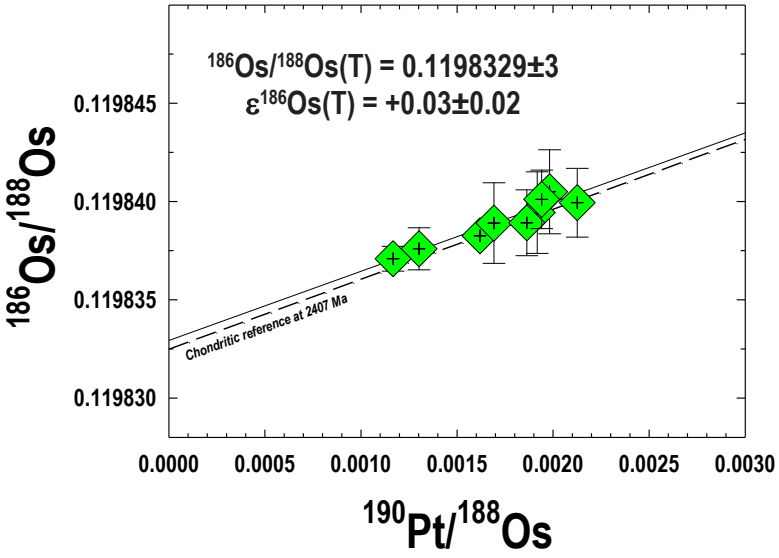

1428

1429 **Fig. 7.**

1430

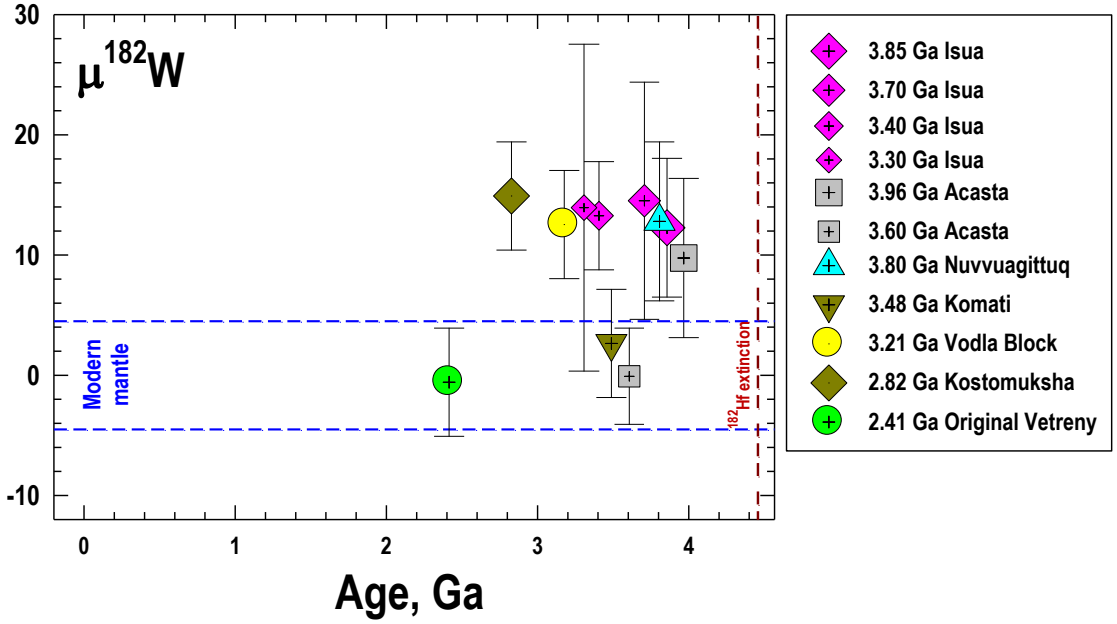

1431

1432 **Fig. 8.**

1433

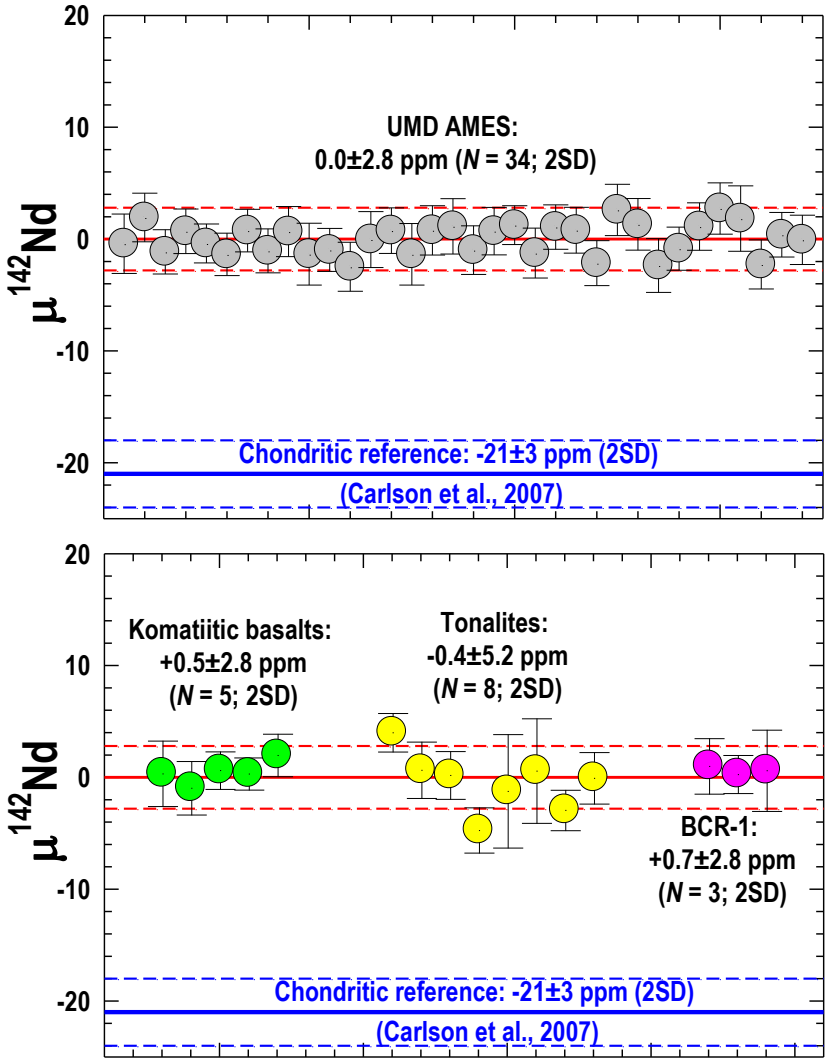
20
10
0
-10
-20
μ142Nd
UMD AMES:
0.0±2.8 ppm (N = 34; 2SD)
Chondritic reference: -21±3 ppm (2SD)
(Carlson et al., 2007)
Komatiitic basalts:
+0.5±2.8 ppm
(N = 5; 2SD)
Tonalites:
-0.4±5.2 ppm
(N = 8; 2SD)
BCR-1:
+0.7±2.8 ppm
(N = 3; 2SD)
Chondritic reference: -21±3 ppm (2SD)
(Carlson et al., 2007)

Fig. 9.

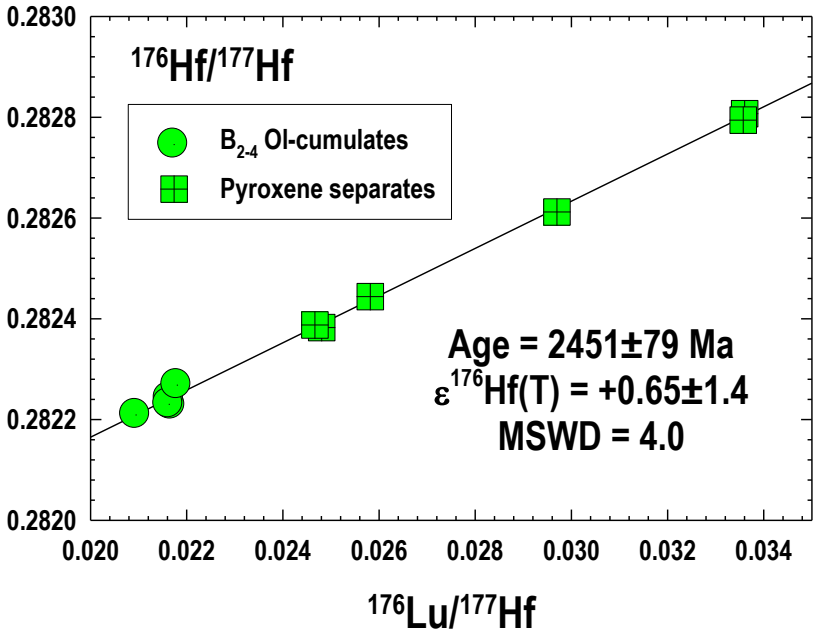

1437

1438 **Fig. 10.**

1439

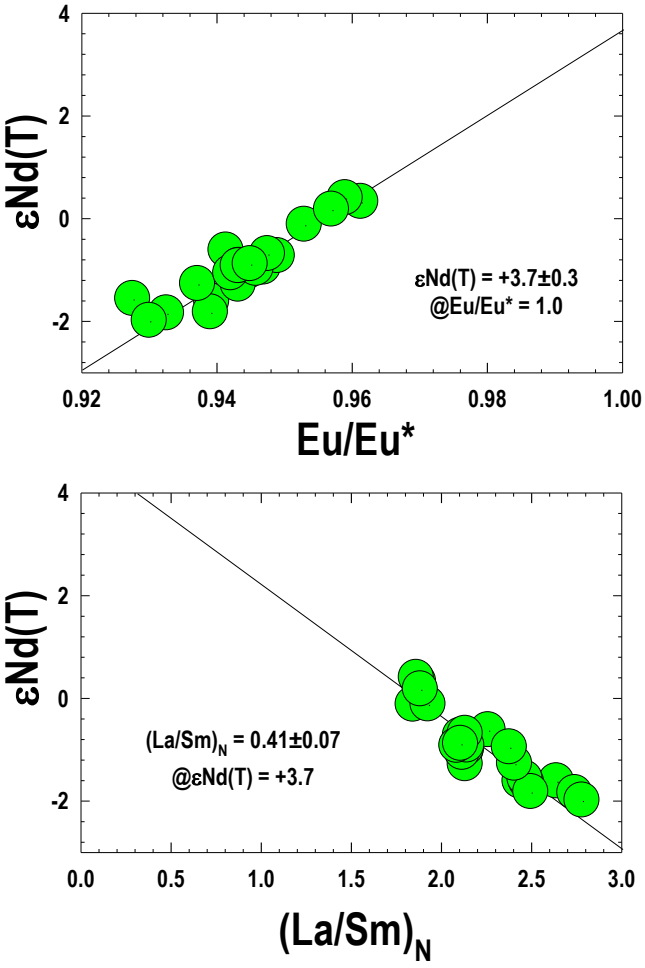

1440

1441 **Fig. 11.**

1442

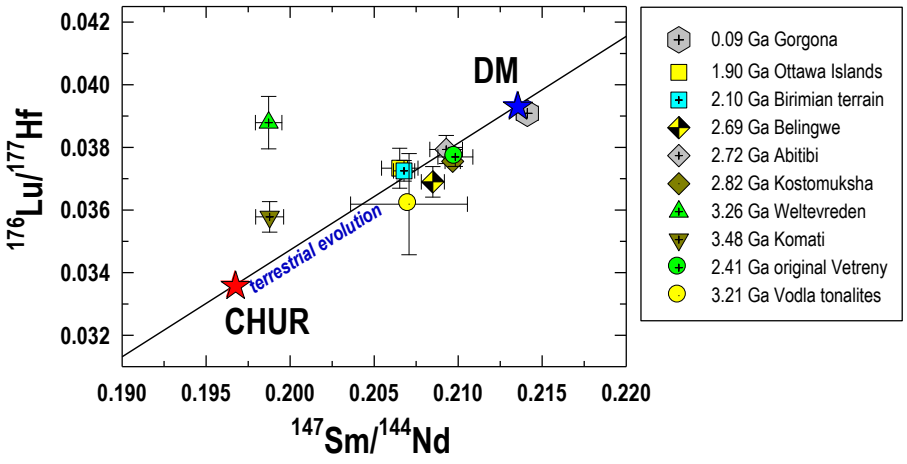

1443

1444 **Fig. 12.**

1445

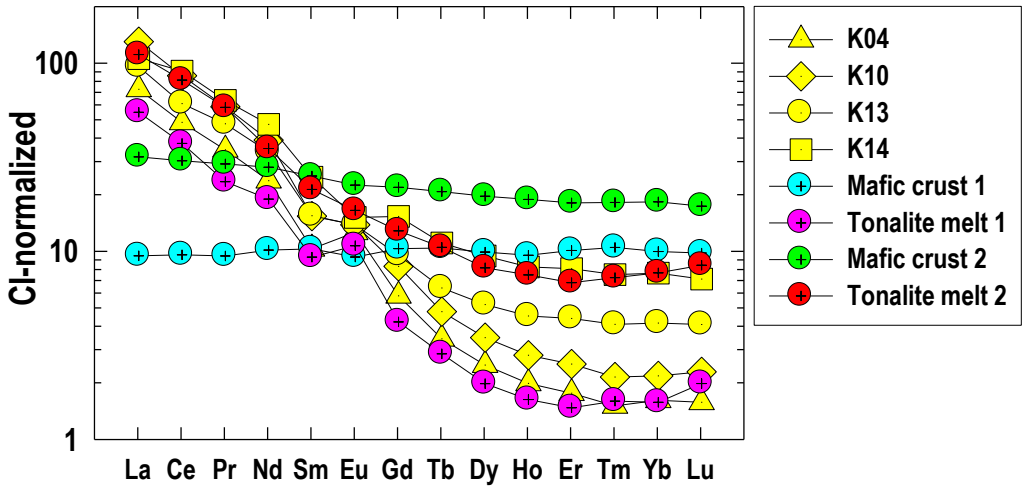

1446

1447 **Fig. 13.**

1448

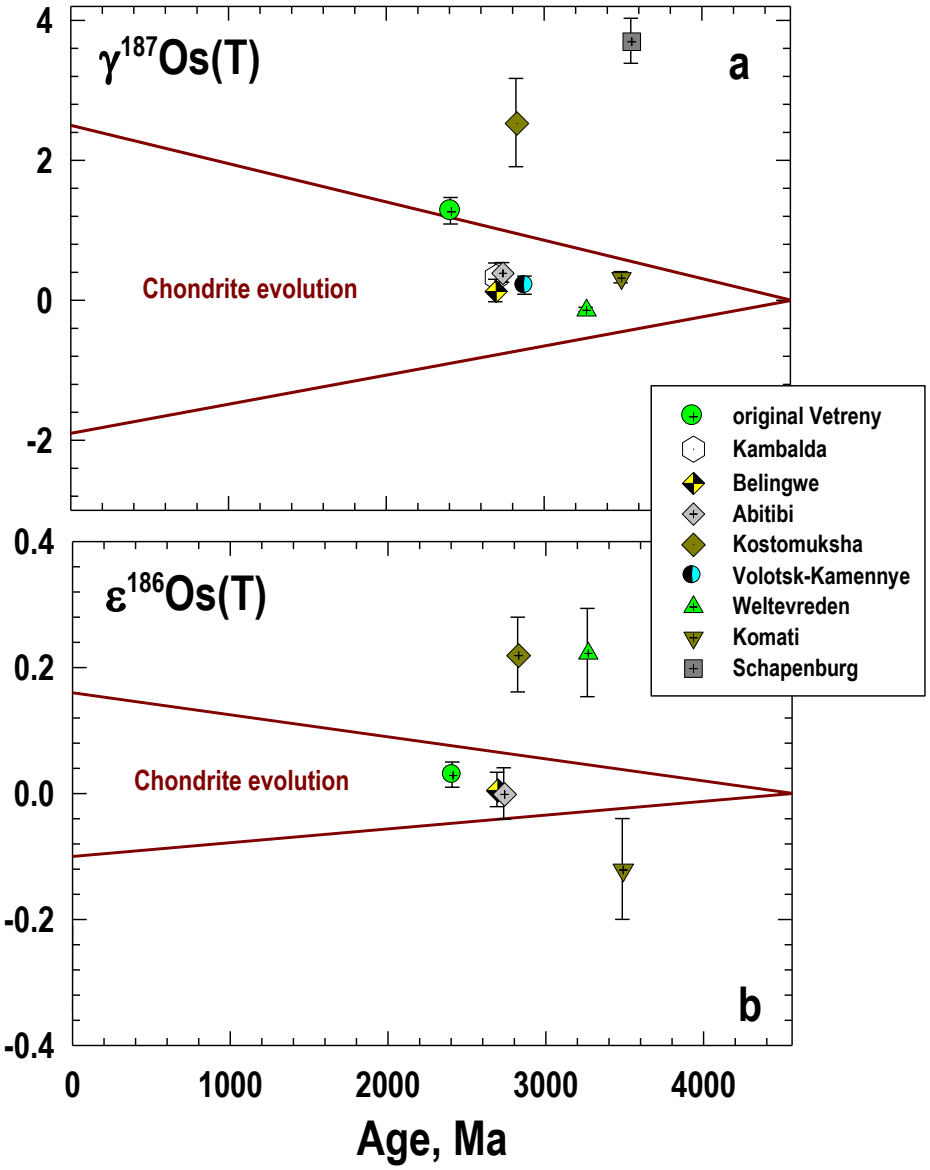

1449

1450 **Fig. 14.**

1451

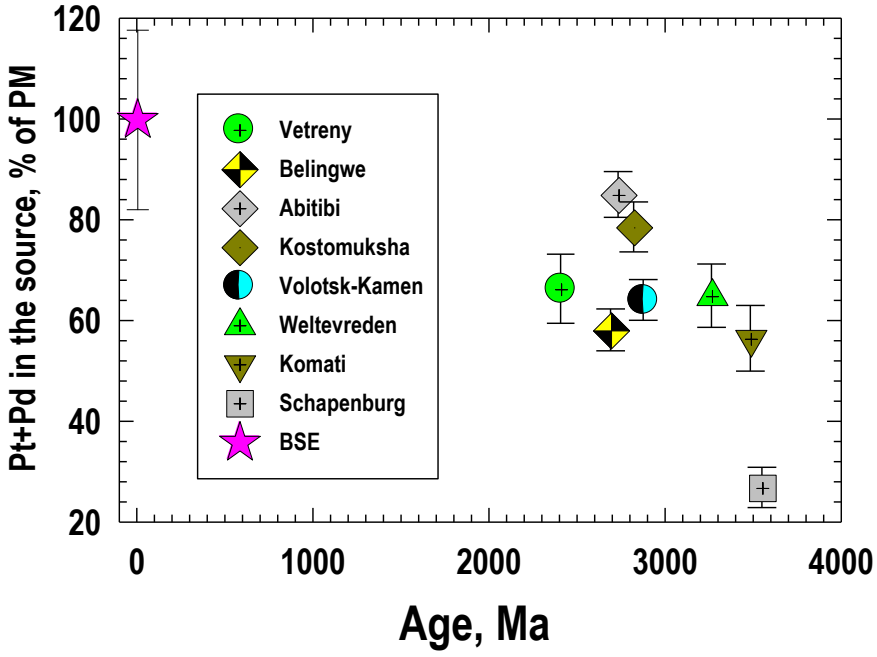

1452

1453

1454 **Fig. 15.**

1455

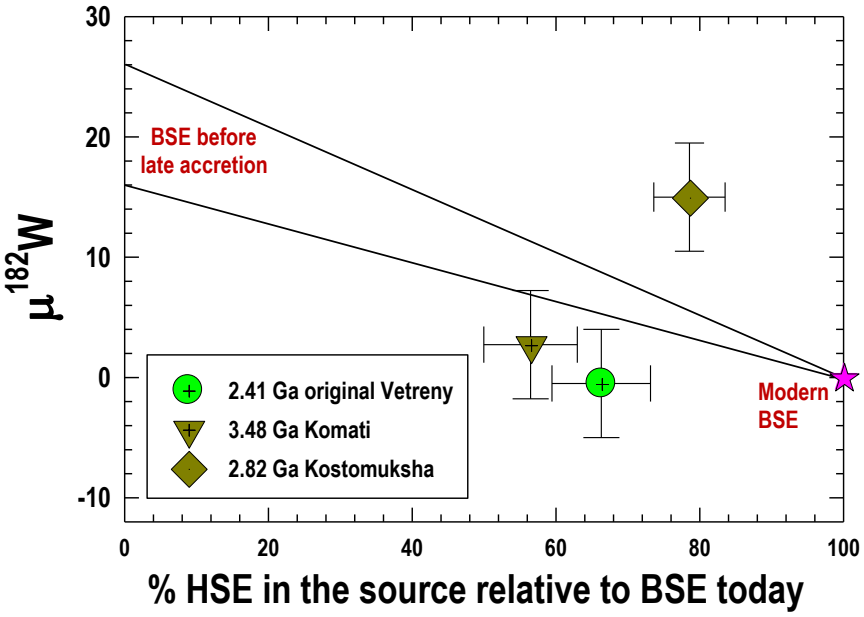

1456

1457 **Fig. 16.**

1458